SMAI-JCM
SMAI Journal of Computational Mathematics

A posteriori error estimates and stopping criteria for space-time domain decomposition for two-phase flow between different rock types

Elyes Ahmed, Sarah Ali Hassan, Caroline Japhet, Michel Kern & Martin Vohralík

Volume 5 (2019), p. 195-227.

<http://smai-jcm.cedram.org/item?id=SMAI-JCM_2019__5__195_0>

SMAI Journal of Computational Mathematics
Vol. 5, 195-227 (2019)

A posteriori error estimates and stopping criteria for space-time domain decomposition for two-phase flow between different rock types

Elyes Ahmed [1]
Sarah Ali Hassan [2]
Caroline Japhet [3]
Michel Kern [4]
Martin Vohralík [5]

[1] Inria, 2 rue Simone Iff, 75589 Paris, France
Current address: Department of Mathematics, University of Bergen, Bergen, Norway
E-mail address: elyes.ahmed@uib.no
[2] Inria, 2 rue Simone Iff, 75589 Paris, France
& Université Paris-Est, CERMICS (ENPC), 77455 Marne-la-Vallée 2, France
E-mail address: sarah.ali-hassan@inria.fr
[3] Université Paris 13, Sorbonne Paris Cité, LAGA, CNRS (UMR 7539), 93430, Villetaneuse, France
E-mail address: japhet@math.univ-paris13.fr
[4] Inria, 2 rue Simone Iff, 75589 Paris, France
& Université Paris-Est, CERMICS (ENPC), 77455 Marne-la-Vallée, France
E-mail address: michel.kern@inria.fr
[5] Inria, 2 rue Simone Iff, 75589 Paris, France
& Université Paris-Est, CERMICS (ENPC), 77455 Marne-la-Vallée, France
E-mail address: martin.vohralik@inria.fr.

Abstract. We consider two-phase flow in a porous medium composed of two different rock types, so that the capillary pressure field is discontinuous at the interface between the rocks. This is a nonlinear and degenerate parabolic problem with nonlinear and discontinuous transmission conditions on the interface. We first describe a space-time domain decomposition method based on the optimized Schwarz waveform relaxation algorithm (OSWR) with Robin or Ventcell transmission conditions. Complete numerical approximation is achieved by a finite volume scheme in space and the backward Euler scheme in time. We then derive a guaranteed and fully computable a posteriori error estimate that in particular takes into account the domain decomposition error. Precisely, at each iteration of the OSWR algorithm and at each linearization step, the estimate delivers a guaranteed upper bound on the error between the exact and the approximate solution. Furthermore, to make the algorithm efficient, the different error components given by the spatial discretization, the temporal discretization, the linearization, and the domain decomposition are distinguished. These ingredients are then used to design a stopping criterion for the OSWR algorithm as well as for the linearization iterations, which together lead to important computational savings. Numerical experiments illustrate the efficiency of our estimates and the performance of the OSWR algorithm with adaptive stopping criteria on a model problem in three space dimensions. Additionally, the results show how a posteriori error estimates can help determine the free Robin or Ventcell parameters.

2010 Mathematics Subject Classification. 65M08, 65M15, 65M50, 65M55, 76S05.

Keywords. two-phase Darcy flow, discontinuous capillary pressure, finite volume scheme, domain decomposition method, optimized Schwarz waveform relaxation, Robin and Ventcell transmission conditions, linearization, a posteriori error estimate, stopping criteria.

This work was funded by the French ANR DEDALES under grant ANR-14-CE23-0005, Labex MME-DII, and the French Agency for Nuclear Waste Management (ANDRA). It also received funding from the European Research Council (ERC) under the European Union's Horizon 2020 research and innovation program (grant agreement No 647134 GATIPOR).

1. Introduction

Two-phase flows in porous media are of interest in many applications, such as CO2 sequestration in saline aquifers, description of oil reservoirs, or gas migration around a nuclear waste repository in the subsurface. The numerical simulation of such flows is a challenging task. One well-known reason, which is the main topic of this paper, is that the capillary pressure and the relative permeability functions may be discontinuous across the interface between different regions of the domain.

We consider in this paper a simplified two-phase flow model (one equation, no advection) introduced in [24] to study the phenomenon of oil or gas trapping in a porous medium with several rock types (see also [14, 52] for the analysis of a 1D model). The main theoretical and numerical difficulties of this problem are the *nonlinearity* and *degeneracy* of the parabolic equation for the saturation of one of the phases, together with *nonlinear* and *discontinuous transmission conditions* at the interface between the rocks. Existence of a weak solution has been proven in [24], using the convergence of a finite volume scheme (see also [17, 18], and [15] for the full two-phase flow model). Uniqueness of a weak solution has been proven in [17] for a particular choice of functions characterizing the porous medium and in [18, 19] for the full two-phase problem with advection terms in the one-dimensional case. An a priori convergence study of a finite volume discretization has been undertaken in [24]. Due to different hydrogeological properties of the different rocks, domain decomposition (DD) methods appear to be a natural way to solve efficiently two-phase flow problems, and are proposed in [55, 56] as well as [31, 39, 48, 49, 50, 51].

The first purpose of this paper is to propose a *domain decomposition method* that is *global-in-time*, with time-dependent, nonlinear, and discontinuous optimized Ventcell transmission conditions at the interface between rock types, for solving the two-phase flow model of [24]. This method is based on the optimized Schwarz waveform relaxation algorithm (OSWR), in which at each OSWR iteration, space-time nonlinear subdomain problems over the whole time interval are solved. The exchange between the subdomains is here ensured using the nonlinear Ventcell transmission operators. Crucially, this approach allows for *different time stepping* in different parts of the domain, adapted to the physical properties of each subdomain, and for *parallelization in time*, in contrast to the domain decomposition algorithms discussed above. We are not aware of any domain decomposition algorithm proposed and analyzed for simultaneously a) degenerate parabolic problems; b) nonlinear and discontinuous transmission conditions; c) Robin and Ventcell transmission conditions; d) global-in-time formulation. Some of these ingredients have appeared previously independently as in [12, 13, 15, 32, 33, 35] and the references therein. The use of higher-order (Ventcell) transmission operators allows physically more valuable information to be exchanged between the subdomains and hence typically leads to a better convergence behavior, see [12, 29, 33, 35, 36, 37, 41] and the references therein for linear problems, and [16, 32] for problems with nonlinear reaction terms. The Robin case, obtained by setting one of the Ventcell parameters to zero, is analyzed in [3, 4], both for the existence of a weak solution of the subdomain problem with Robin boundary conditions, and to prove that the space-time DD method is well-defined.

The second purpose of this paper is to derive *a posteriori error estimates* for the finite volume – backward Euler approximation of the proposed space-time DD algorithm. We build here on the (few) previous contributions on unsteady, nonlinear, and degenerate problems in [20, 23, 42]; we will in particular rely on [23, Theorem 5.2], where the degenerate nature of the problem is handled to obtain an energy-type upper bound on the error. Two additional specific difficulties that were to the best of our knowledge not treated previously are that the current problem features nonlinear and discontinuous transmission conditions and that our finite volume discretization leads to an approximate solution that is nonconforming in space.

Finally, the third purpose of this paper is to address the question of when to *stop* the domain decomposition *iterations*, as well as the iterations of the linearization solver used for the subdomain

problems. In contrast to prevalent practice, where one iterates until some fixed tolerance has been reached, we propose to stop when the DD/linearization error component is up to a user-specified fraction below the total error. This typically spares numerous iterations. In practice, this means that the a posteriori error estimates we develop have to hold true at *each iteration* of the OSWR algorithm and the linearization, and distinguish the different error components (space, time, linearization, and domain decomposition). For this part of our work, we take up the path initiated in [9, 11, 26, 38, 54] for general techniques taking into account inexact algebraic solvers, [45] for (multiscale) mortar techniques, [46, 47] for FETI and BDD domain decomposition algorithms combined with conforming finite element discretizations, and most closely [6, 7] for respectively steady and unsteady linear problems with similar space and time discretizations. To achieve our goals here, we use a) equilibrated $\mathbf{H}(\mathrm{div})$-conforming flux reconstructions, piecewise constant in time, that are direct extension of [7, 25, 54] to our model; b) novel subdomain-wise H^1-conforming saturation reconstructions, continuous and piecewise affine in time, which are targeted to the present setting in that they satisfy the nonlinear and discontinuous interface conditions.

The outline of the paper is as follows: Section 2 recalls the physical model and defines weak solutions as well as the relevant functions spaces. Section 3 presents the space-time domain decomposition method with nonlinear and discontinuous Ventcell transmission conditions. In Section 4, we present the discrete OSWR algorithm, by combining a finite volume scheme for the discretization in the individual subdomains and the backward Euler time stepping with the OSWR method. We then construct the needed ingredients for the a posteriori error estimates: Section 5 defines the postprocessing as well as the H^1- and $\mathbf{H}(\mathrm{div})$-conforming reconstructions. Section 6 puts the pieces together by presenting a guaranteed and fully computable error estimate that bounds the error between the unknown exact solution and the approximate solution. In Section 7 we decompose this overall estimator into individual estimators characterizing the space, time, domain decomposition, and linearization error components. This is used in Section 8 to propose stopping criteria for the OSWR algorithm and for the nonlinear iterations. The method is numerically validated on three examples in three space dimensions in Section 9. Finally, Section 10 draws some conclusions.

2. Presentation of the problem

Let Ω be an open bounded domain of $\mathbb{R}^d$, $d = 2$ or 3, which is assumed to be polygonal if $d = 2$ and polyhedral if $d = 3$. We denote by $\partial\Omega$ its boundary (supposed to be Lipschitz-continuous) and by $\mathbf{n}$ the unit normal to $\partial\Omega$, outward to Ω. Let a time interval $(0, T)$ be given with $T > 0$. We consider a simplified model of a two-phase flow through a heterogeneous porous medium, in which the advection is neglected. Assuming that there are only two phases occupying the porous medium Ω, say gas and water, and that each phase is composed of a single component, the mathematical form of this problem as it is presented in [17, 24] is as follows: given initial and boundary gas saturations u_0 and g, as well as a source term f, find $u : \Omega \times [0, T] \to [0, 1]$ such that

$$\partial_t u - \nabla\cdot(\lambda(u, \mathbf{x})\nabla\pi(u, \mathbf{x})) = f, \quad \text{in } \Omega \times (0, T), \tag{2.1a}$$

$$u(\cdot, 0) = u_0, \quad \text{in } \Omega, \tag{2.1b}$$

$$u = g, \quad \text{on } \partial\Omega \times (0, T). \tag{2.1c}$$

Here u is the *gas saturation* (and therefore $(1 - u)$ is the water saturation), $\pi(u, \mathbf{x}) : [0, 1] \times \Omega \to \mathbb{R}$ is the *capillary pressure*, and $\lambda(u, \mathbf{x}) : [0, 1] \times \Omega \to \mathbb{R}$ is the *global mobility* of the gas given by

$$\lambda(u) = \frac{\lambda_{\mathrm{w}}(1 - u)\lambda_{\mathrm{g}}(u)}{\lambda_{\mathrm{w}}(1 - u) + \lambda_{\mathrm{g}}(u)},$$

where λ_w and λ_g are the phase mobilities. One can refer to [20, 21, 24] for a derivation of (2.1a)– (2.1c) from the complete two-phase flow model. For simplicity, we consider only Dirichlet boundary conditions on $\partial\Omega$. Other types of boundary conditions could be dealt with the same way as in [17, 24, 54]. The model problem given by (2.1a) is a nonlinear degenerate parabolic problem as the global mobility $\lambda(u) \to 0$ for $u \to 0$ and 1, and, moreover, $\pi'(u) \to 0$ for $u \to 0$ (see [10, 21]).

2.1. **Flow between two rock types**

In this part, we particularize the model problem (2.1a) to a porous medium with different capillary pressure curves π_i in each subdomain, following [24]. We suppose that Ω is composed of two disjoint subdomains Ω_i, $i = 1, 2$, which are both open polygonal subsets of $\mathbb{R}^d$ with Lipschitz-continuous boundary. We denote by Γ the interface between Ω_1 and Ω_2, i.e., $\Gamma = (\partial\Omega_1 \cap \partial\Omega_2)^\circ$. Let $\Gamma_i^{\mathrm{D}} = \partial\Omega_i \cap \partial\Omega$. Both data λ and π, which can in general depend on the physical characteristics of the rock, are henceforth supposed to be homogeneous in each subdomain Ω_i, $i = 1, 2$, i.e., $\lambda_i(\cdot) := \lambda_{|\Omega_i}(\cdot) = \lambda(\cdot, \mathbf{x}), \forall \mathbf{x} \in \Omega_i$, and similarly for π_i. Equations (2.1a) in *each subdomain* Ω_i then read as

$$\partial_t u_i - \nabla\cdot(\lambda_i(u_i)\nabla\pi_i(u_i)) = f_i, \quad \text{in } \Omega_i \times (0,T), \tag{2.2a}$$

$$u_i(\cdot, 0) = u_0, \quad \text{in } \Omega_i, \tag{2.2b}$$

$$u_i = g_i, \quad \text{on } \Gamma_i^{\mathrm{D}} \times (0,T). \tag{2.2c}$$

We use the notation $v_i = v|_{\Omega_i}$ for an arbitrary function v.

Before transcribing the transmission conditions on the interface Γ, we make precise the assumptions on the data (further generalizations are possible, bringing more technicalities):

Assumption 2.1 (Data)**.** *(1) For $i \in \{1, 2\}$, $\pi_i \in C^1([0, 1], \mathbb{R})$ can be extended in a continuous way to a function (still denoted by π_i) such that $\pi_i(u) = \pi_i(0)$ for all $u \le 0$ and $\pi_i(u) = \pi_i(1)$ for all $u \ge 1$. Moreover, $\pi_i|_{[0,1]}$ is a strictly increasing function.*

(2) For $i \in \{1, 2\}$, $\lambda_i \in C^0([0, 1], \mathbb{R}^+)$ is bounded and can be extended in a continuous way to a function (still denoted by λ_i) such that $\lambda_i(u) = \lambda_i(0)$ for all $u \le 0$ and $\lambda_i(u) = \lambda_i(1)$ for all $u \ge 1$. We denote by C_λ an upper bound of $\lambda_i(u)$, $u \in \mathbb{R}$.

(3) The initial condition is such that $u_0 \in L^\infty(\Omega)$ with $0 \le u_0 \le 1$ a.e. in Ω.

(4) The boundary conditions $0 \le g_i \le 1$ are traces of some functions in $L^2(0, T; H^1(\Omega_i))$. For simplicity, we suppose them to be at most piecewise second-order polynomials with respect to the boundary faces of the spatial mesh introduced in Section 4.1.1 below, continuous on Γ_i^{D}, and constant in time. Moreover, they need to match in the sense that $\pi_1(g_1(\mathbf{x})) = \pi_2(g_2(\mathbf{x}))$ for all $\mathbf{x} \in \Gamma \cap \Gamma_1^{\mathrm{D}} \cap \Gamma_2^{\mathrm{D}}$.

(5) The source term is such that $f \in L^2(0, T; L^2(\Omega))$. For simplicity we further assume that f is piecewise constant in time with respect to the temporal mesh introduced in Section 4.1.2 below.

For simplicity, we suppose in Assumption 2.1(4) that the boundary conditions are piecewise polynomial in space and constant in time, so that there is in particular no additional data oscillation error stemming therefrom.

We give now the *transmission conditions* needed to connect the subdomain problems (2.2), for $i = 1, 2$. We consider two cases. The first case is when

$$\pi_1(0) = \pi_2(0) \qquad \text{and} \qquad \pi_1(1) = \pi_2(1), \tag{2.3}$$

the same way as in [17]. If the functions π_i satisfy the above condition, the capillarity curves are said to be matching and the resulting transmission conditions on the interface are given by

$$\pi_1(u_1) = \pi_2(u_2), \qquad \text{on } \Gamma \times (0,T), \tag{2.4a}$$

$$\lambda_1(u_1)\nabla\pi_1(u_1)\cdot\mathbf{n}_1 = -\lambda_2(u_2)\nabla\pi_2(u_2)\cdot\mathbf{n}_2, \quad \text{on } \Gamma \times (0,T). \tag{2.4b}$$

These conditions yield a discontinuous saturation across the interface, i.e., we find that in general $u_1 \neq u_2$ on Γ.

In the second case, i.e., in the case when

$$\pi_1(0) \neq \pi_2(0) \qquad \text{or} \qquad \pi_1(1) \neq \pi_2(1), \tag{2.5}$$

the capillarity pressure curves are said to be non-matching. Consequently, not only the saturation is discontinuous at the medium interface, but also the capillary pressure field. The condition (2.5), studied in [24], has direct consequences on the behavior of the capillary pressures on both sides of the interface Γ. Indeed, suppose that $\pi_1(0) \leq \pi_2(0) < \pi_1(1) \leq \pi_2(1)$, that u_1^* is the unique real in $[0,1]$ satisfying $\pi_1(u_1^*) = \pi_2(0)$, and that u_2^* is the unique real in $[0,1]$ satisfying $\pi_2(u_2^*) = \pi_1(1)$. Then, if $u_1 \geq u_1^*$ and $u_2 \leq u_2^*$, we can still prescribe the connection of the capillary pressures on the interface Γ $\pi_1(u_1) = \pi_2(u_2)$ as in (2.4a). If $0 \leq u_1 \leq u_1^*$, the model imposes $u_2 = 0$, and the gas phase is entrapped in the rock Ω_1 while the water flows across Γ. In the same way, if $u_2^* \leq u_2 \leq 1$, the model prescribes $u_1 = 1$, and the water phase is captured in Ω_2 as a discontinuous phase while the gas flows across Γ (see Fig. 2.1 left). Following [21, 24], these conditions on the gas-water saturations on the interface Γ are simply given by

$$\overline{\pi}_1(u_1) = \overline{\pi}_2(u_2), \qquad \text{on } \Gamma \times (0,T), \tag{2.6a}$$

$$\lambda_1(u_1)\nabla\pi_1(u_1)\cdot\mathbf{n}_1 = -\lambda_2(u_2)\nabla\pi_2(u_2)\cdot\mathbf{n}_2, \quad \text{on } \Gamma \times (0,T), \tag{2.6b}$$

where $\overline{\pi}_i$, for $i = 1, 2$, are truncated capillary pressure functions given on $[0,1]$ respectively by $\overline{\pi}_1 : u \mapsto \max(\pi_1(u), \pi_2(0))$ and $\overline{\pi}_2 : u \mapsto \min(\pi_2(u), \pi_1(1))$ (see Fig. 2.1 right). In [24], it has been established that the model problem (2.2) together with the transmission conditions (2.6) has the necessary mathematical properties to explain the phenomena of gas trapping (see also [14, 8, 19, 52]).

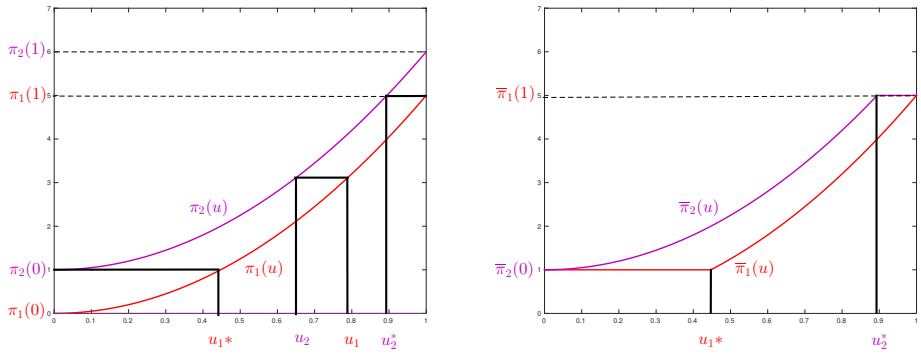

FIGURE 2.1. Capillary pressure curves (left) and truncated capillary pressures curves (right)

2.2. **Transformation of the equations and weak formulation**

Still following [24], we present here the mathematical quantities and function spaces used to characterize the weak solution to the multidomain problem (2.2) with the conditions (2.6). That of the problem (2.2) with the conditions (2.4) can be deduced straightforwardly from this later, see [17]. As

Ω_i is a homogeneous rock type, so that π_i and λ_i do not depend on $\mathbf{x}$, one can define the Kirchhoff transform in each subdomain

$$\varphi_i : \left\{ \begin{array}{ccc} [0,1] & \longrightarrow & \mathbb{R}^+ \\ s & \longmapsto & \int_0^s \lambda_i(a)\pi_i'(a)\mathrm{d}a. \end{array} \right. \tag{2.7}$$

The function φ_i is Lipschitz-continuous and increasing on $[0,1]$, and we denote by $L_{\varphi,i}$ its Lipschitz constant, i.e., $L_{\varphi,i} := \max_{s\in[0,1]} \lambda_i(s)\pi_i'(s)$, so that

$$|\varphi_i(a) - \varphi_i(b)| \leq L_{\varphi,i}|a-b|, \quad \forall (a,b) \in [0,1]^2,$$

and we let $L_\varphi := \max(L_{\varphi,1}, L_{\varphi,2})$. We extend the function φ_i from $[0,1]$ to $\mathbb{R}$ so that $\varphi_i(u) = \varphi_i(0)$ for all $u \leq 0$ and $\varphi_i(u) = \varphi_i(1)$ for all $u \geq 1$.

We now introduce the strictly increasing function ϕ by

$$\phi : \left\{ \begin{array}{ccc} [\pi_2(0), \pi_1(1)] & \longrightarrow & \mathbb{R}^+ \\ s & \longmapsto & \displaystyle\int_{\pi_2(0)}^{s} \min_{j\in\{1,2\}} (\lambda_j \circ \pi_j^{-1}(a))\,\mathrm{d}a, \end{array} \right.$$

and let $\Pi_i := \phi \circ \overline{\pi}_i$, for $i \in \{1,2\}$. The functions $\Pi_i|_{[0,1]}$, introduced first in [24, Lemma 1.2] and used in [4, 3, 17, 19], are differentiable and increasing. We let $\Pi_i(u) = \Pi_i(0)$ for all $u \leq 0$ and $\Pi_i(u) = \Pi_i(1)$ for all $u \geq 1$ and define the function Π by

$$\Pi(u, \mathbf{x}) = \Pi_i(u), \quad \text{for } \mathbf{x} \in \Omega_i.$$

As Π_i are more regular than $\overline{\pi}_i$, this allows to connect Π_1 and Π_2 instead of $\overline{\pi}_1$ and $\overline{\pi}_2$, that is, for all $(u_1, u_2) \in \mathbb{R}^2$, we have the crucial *equivalence property*

$$\overline{\pi}_1(u_1) = \overline{\pi}_2(u_2) \Leftrightarrow \Pi_1(u_1) = \Pi_2(u_2).$$

Finally, under Assumption 2.1, the function $\Pi_i \circ \varphi_i^{-1}$ is Lipschitz-continuous with a Lipschitz constant lower than 1 (see [24, Lemma 1.2]), i.e.

$$|\Pi_i(a) - \Pi_i(b)| \leq |\varphi_i(a) - \varphi_i(b)|, \quad \forall (a,b) \in [0,1]^2. \tag{2.8}$$

This inequality will be used in Remark 6.3 below.

We now apply the Kirchhoff transformation (2.7) separately in each subdomain, giving an equivalent formulation suitable for *mathematical analysis*: find u_i such that

$$\partial_t u_i - \Delta\varphi_i(u_i) = f_i, \qquad \text{in } \Omega_i \times (0,T), \tag{2.9a}$$

$$u_i(\cdot, 0) = u_0, \qquad \text{in } \Omega_i, \tag{2.9b}$$

$$\varphi_i(u_i) = \varphi_i(g_i), \quad \text{on } \Gamma_i^{\mathrm{D}} \times (0,T), \tag{2.9c}$$

together with the conditions at the interface relying on the smoother functions Π_i

$$\Pi_1(u_1) = \Pi_2(u_2), \qquad \text{on } \Gamma \times (0,T), \tag{2.10a}$$

$$\nabla\varphi_1(u_1)\cdot\mathbf{n}_1 = -\nabla\varphi_2(u_2)\cdot\mathbf{n}_2, \quad \text{on } \Gamma \times (0,T). \tag{2.10b}$$

In general, the multidomain problem (2.9)–(2.10) does not have any strong solution, but the introduction of the Kirchhoff transforms φ_i and of the smoother functions Π_i will, following [24], allow for a definition of a weak solution. To this aim, we define

$$X_{\varphi_i(g_i)} := L^2(0,T; H^1_{\varphi_i(g_i)}(\Omega_i)),$$

$$X_{\Pi(g,\cdot)} := L^2(0,T; H^1_{\Pi(g,\cdot)}(\Omega)), \qquad X := L^2(0,T; H^1_0(\Omega)),$$

where $H^1_{\varphi_i(g_i)}(\Omega_i) := \{v \in H^1(\Omega_i), v = \varphi_i(g_i) \text{ on } \Gamma_i^{\mathrm{D}}\}$ and similarly $H^1_{\Pi(g,\cdot)}(\Omega) := \{v \in H^1(\Omega), v = \Pi(g,\cdot) \text{ on } \partial\Omega\}$.

We equip the space X with the norm

$$||\psi||_X := \left\{ \int_0^T ||\nabla\psi(\cdot,t)||^2_{L^2(\Omega)} \,\mathrm{d}t \right\}^{\frac{1}{2}}.$$

The dual space of X is

$$X' := L^2(0,T;H^{-1}(\Omega)). \tag{2.11}$$

We will use the notation $\langle\cdot,\cdot\rangle_{H^{-1}(\Omega),H^1_0(\Omega)}$ to denote the duality pairing between $H^{-1}(\Omega)$ and $H^1_0(\Omega)$. We will also need the space

$$Z := H^1(0,T;H^{-1}(\Omega)).$$

Using the above developments, a *weak solution* to problem (2.9)–(2.10) is defined as:

Definition 2.2 (Weak solution)**.** *We say that a function u is a weak solution to problem* (2.9)–(2.10) *if it satisfies:*

(1) $u \in Z$*;*

(2) $u(\cdot,0) = u_0$*;*

(3) $\varphi_i(u_i) \in X_{\varphi_i(g_i)}$*, where* $u_i := u|_{\Omega_i}$*,* $i = 1,2$*;*

(4) $\Pi(u,\cdot) \in X_{\Pi(g,\cdot)}$*;*

(5) For all $\psi \in X$*, the following integral equality holds:*

$$\int_0^T \Big\{ \langle \partial_t u, \psi\rangle_{H^{-1}(\Omega),H^1_0(\Omega)} + \sum_{i=1}^{2} (\nabla\varphi_i(u_i), \nabla\psi)_{\Omega_i} - (f,\psi) \Big\}\mathrm{d}t = 0. \tag{2.12}$$

In this paper, we assume that a weak solution given by Definition 2.2 exists. One can then easily show that Π has sufficient regularity to impose the condition (2.10a). Indeed, since $\Pi_i \circ \varphi_i^{-1}$ is a Lipschitz-continuous function, the third point of Definition 2.2 ensures that $\Pi_i(u_i)$ belongs to $L^2(0,T;H^1(\Omega_i))$, $i = 1,2$. Thus, the point 4 of Definition 2.2 implies the continuity condition (2.10a). Finally, when supposing additionally that the weak solution u is sufficiently regular so that $\partial_t u \in L^2(0,T;L^2(\Omega))$, condition (2.10b) is satisfied weakly using point 5 of Definition 2.2.

Remark 2.3 (Existence and uniqueness of a weak solution)**.** *In* [24]*, the existence of a weak solution to problem* (2.9)–(2.10) *(with homogeneous Neumann boundary conditions) was proved using integration by parts for the time term which requires a stronger test function space. Using the imposed conditions, one also finds* $u \in L^\infty(0,T;L^\infty(\Omega))$*, with* $0 \le u \le 1$ *a.e. in* $\Omega \times (0,T)$*. In fact, in* [24] *(see also* [17]*), the derived weak solution is given as the limit of a finite volume approximation of the solution refining the space and time discretization, and requires a stronger test function space for the application of the Kolmogorov compactness criterion in* L^∞*. For the uniqueness, a first result was obtained in* [17] *for the case of matching capillary pressures curves. For the more general case, the uniqueness is demonstrated only for the one-dimensional case in* [18]*.*

3. Space-time domain decomposition with Ventcell transmission conditions

This section proposes our global-in-time domain decomposition method for the degenerate parabolic problem (2.9) with the nonlinear and discontinuous interface conditions (2.10). We in particular design appropriate Robin and Ventcell transmission conditions.

An equivalent formulation to the model problem (2.9)–(2.10) can be obtained by solving, for $i = 1, 2$, equations (2.9) together with optimized Ventcell transmission conditions on $\Gamma \times (0, T)$

$$\nabla\varphi_1(u_1)\cdot\mathbf{n}_1 + \mathcal{L}_1(\Pi_1(u_1)) = -\nabla\varphi_2(u_2)\cdot\mathbf{n}_2 + \mathcal{L}_1(\Pi_2(u_2)), \tag{3.1a}$$

$$\nabla\varphi_2(u_2)\cdot\mathbf{n}_2 + \mathcal{L}_2(\Pi_2(u_2)) = -\nabla\varphi_1(u_1)\cdot\mathbf{n}_1 + \mathcal{L}_2(\Pi_1(u_1)), \tag{3.1b}$$

where $\mathcal{L}_i$, $i = 1, 2$, is a *Ventcell* (or second-order) *boundary operator* defined by

$$\mathcal{L}_i(v) := \alpha_{i,j}v + \gamma_{i,j}(\partial_t v - \Delta_\Gamma v), \quad j = (3 - i), \tag{3.2}$$

for a sufficiently regular function v defined on $\Gamma \times (0, T)$, where Δ_Γ represents the Laplace operator on Γ (the Laplace–Beltrami operator), and $\alpha_{i,j}$ and $\gamma_{i,j}$ are free parameters that can be chosen so as to optimize the convergence factor of the algorithm (see Remark 3.1 below). A sufficient condition for the equivalence of (2.10) and (3.1) to hold is $\alpha_{i,j} > 0$ and $\gamma_{i,j} \geq 0, j = 3 - i,\ i = 1, 2$. The *Robin transmission conditions* are simply obtained by taking in (3.2) the parameters $\gamma_{i,j} = 0$. One can easily show that the operators $\mathcal{L}_i$ involve not only the continuity of the function Π as for the Robin case, but also the continuity of the time derivative and of the second-order derivatives of Π along the interface. As a result, this formulation can be seen as a coupling problem between a d-dimensional PDE in the rock Ω_i and a $(d-1)$-dimensional PDE on the interface Γ between the rock types, which greatly enhances the information exchange between the solutions in the subdomains, see [16, 29, 33, 37] for some model cases.

The Ventcell–OSWR algorithm is defined as follows: the solution u in the whole domain Ω given by $u_i = u|_{\Omega_i}$ is approximated by a sequence of solutions u_i^k, $k \geq 1$, defined recursively by solving by

$$\partial_t u_i^k - \Delta\varphi_i(u_i^k) = f_i, \qquad \text{in } \Omega_i \times (0, T), \tag{3.3a}$$

$$u_i^k(\cdot, 0) = u_0, \qquad \text{in } \Omega_i, \tag{3.3b}$$

$$\varphi_i(u_i^k) = \varphi_i(g_i), \qquad \text{on } \Gamma_i^{\mathrm{D}} \times (0, T), \tag{3.3c}$$

$$\nabla\varphi_i(u_i^k)\cdot\mathbf{n}_i + \mathcal{L}_i(\Pi_i(u_i^k)) = \Psi_i^{k-1}, \qquad \text{on } \Gamma \times (0, T), \tag{3.3d}$$

with

$$\Psi_i^{k-1} := -\nabla\varphi_j(u_j^{k-1})\cdot\mathbf{n}_j + \mathcal{L}_i(\Pi_j(u_j^{k-1})), \quad j = (3 - i),\ k \geq 2, \tag{3.4}$$

and Ψ_i^0 is an initial Ventcell guess on $\Gamma \times (0, T)$.

A proof of existence of a (suitably defined weak) solution of (3.3) can be found in [4] for the case of Robin boundary conditions.

Remark 3.1 (Optimized parameters)**.** *"Optimized parameters" refers to a general way of a priori choosing the Robin or Ventcell parameters $\alpha_{i,j}$ and $\gamma_{i,j}$ in the OSWR methods so as to numerically minimize the convergence factor for a usually simplified (linearized) problem. Here, these parameters are fixed throughout the OSWR iterations by the optimization as in* [29, 33, 37] *for domain decomposition in space, in* [12, 30, 35, 36, 41] *for space-time domain decomposition, and in* [16] *for semilinear problems. These optimized values are represented by the black boxes in Figure 9.3 (left) and Figure 9.8, and we observe that they are not far from the optimal numerical values. The a posteriori analysis and the stopping criteria in this paper are not affected by the specific values of these parameters.*

Remark 3.2 (Interface operators)**.** *The multi-domain problem* (2.9) *together with the transmission conditions* (3.1) *can be formulated through the use of interface operators as a problem posed on the space-time interface, see* [4]*, where Robin-to-Robin conditions are analyzed, and also* [35, 36]*. This interface problem can be solved iteratively by using fixed point iterations (which corresponds to the OSWR algorithm above) or via a Newton–Krylov method.*

Remark 3.3 (Domain decomposition algorithm in physical variables)**.** *The algorithm* (3.3)–(3.4) *is written in the variables* $\varphi_i(u_i^k)$ *and* $\Pi_i(u_i^k)$ *stemming from the rewriting* (2.9)–(2.10) *and the corresponding weak formulation of Definition 2.2. One could also formulate a Ventcell–OSWR domain decomposition algorithm directly in the physical variables, using the original formulation* (2.2) *and the corresponding transmission conditions* (2.6)*:*

$$\partial_t u_i^k - \nabla\cdot\left(\lambda_i(u_i^k)\nabla\pi_i(u_i^k)\right) = f_i, \qquad \text{in } \Omega_i\times(0,T), \tag{3.5a}$$

$$u_i^k(\cdot,0) = u_0, \qquad \text{in } \Omega_i, \tag{3.5b}$$

$$u_i^k = g_i, \qquad \text{on } \Gamma_i^{\mathrm{D}}\times(0,T), \tag{3.5c}$$

$$\lambda_i(u_i^k)\nabla\pi_i(u_i^k)\cdot\mathbf{n}_i + \overline{\mathcal{L}}_i(u_i^k) = \Psi_i^{k-1}, \qquad \text{on } \Gamma\times(0,T), \tag{3.5d}$$

with

$$\begin{aligned}
\overline{\mathcal{L}}_i(u_i^k) &:= \alpha_{i,j}\overline{\pi}_i(u_i^k) + \gamma_{i,j}\left(\partial_t u_i^k - \nabla_\Gamma\cdot\left(\lambda_i(u_i^k)\nabla_\Gamma\pi_i(u_i^k)\right)\right), \quad j=(3-i),\\
\Psi_i^{k-1} &:= -\lambda_j(u_j^{k-1})\nabla\pi_j(u_j^{k-1})\cdot\mathbf{n}_j + \overline{\mathcal{L}}_i(u_i^k), \quad j=(3-i),\ k\geq 2,
\end{aligned} \tag{3.6}$$

where ∇_Γ *and* $\nabla_\Gamma\cdot$ *are respectively the surface gradient and divergence on* Γ *and* Ψ_i^0 *is an initial Ventcell guess on* $\Gamma\times(0,T)$*.*

Though algorithms (3.3)–(3.4) *and* (3.5)–(3.6) *may differ, an a posteriori error analysis of both algorithms can be done simultaneously as in* [20]*, see the "mathematical" scheme of Definition 4.1 and the "engineering" scheme of Definition 4.4 therein. Indeed,* [20, Theorem 3.3] *applies to both schemes. We avoid this here for the sake of conciseness.*

4. Cell-centered finite volume scheme

We present here a finite volume discretization of the OSWR algorithm (3.3)–(3.4); we also develop linearization of the subdomain problems by the Newton method, used later in the a posteriori analysis.

4.1. Space-time discretization, notations, and function spaces

We introduce here partitions of Ω and Γ, time discretization, and discrete function spaces.

4.1.1. *Partitions of* Ω *and* Γ

Let $\mathcal{T}_{h,i}$ be a partition of the subdomain Ω_i into elements K, such that $\overline{\Omega_i} = \cup_{K\in\mathcal{T}_{h,i}}K$; here we suppose that the elements are either simplices or rectangular parallelepipeds but general elements can be treated via submeshes, see [22] and the references therein. Moreover, we assume that the partition is conforming in the sense that if K, $L\in\mathcal{T}_{h,i}$, $K\neq L$, then $K\cap L$ is either an empty set, a common face, edge, or vertex of K and L.

We then set $\mathcal{T}_h = \cup_{i=1}^2\mathcal{T}_{h,i}$ and denote by h the maximal element diameter in $\mathcal{T}_h$. The meshes are supposed to be matching on the interface Γ. For all $K\in\mathcal{T}_h$, h_K denotes the diameter of the mesh element K and $|K|$ its volume. The interior mesh faces in $\mathcal{T}_{h,i}$ are collected into the set $\mathcal{F}_{h,i}^{\mathrm{int}}$; hence $\mathcal{F}_{h,i}^{\mathrm{int}}$ contains neither the subdomain interfaces nor the outer boundary of Ω. The faces of $\mathcal{T}_{h,i}$ lying on Γ_i^{D} are collected in the set $\mathcal{F}_{h,i}^{\mathrm{D}}$. We denote by $\mathcal{F}_{h,i}$ all the faces of $\mathcal{T}_{h,i}$ and we set $\mathcal{F}_h = \cup_{i=1}^2\mathcal{F}_{h,i}$. The notation $\mathcal{F}_K$ stands for all the faces of an element $K\in\mathcal{T}_h$. Let $\mathcal{F}_h^\Gamma$ be a partition of Γ given by the faces of $\mathcal{T}_h$ on Γ. We use also $\mathcal{E}_{h,i}^{\mathrm{int}}$ to denote the interior edges (if $d=3$, or points if $d=2$). We denote by $\mathcal{E}_{h,i}^{\mathrm{D}}$ the edges of $\mathcal{F}_h^\Gamma$ on Γ_i^{D}. The edges of a face $\sigma\in\mathcal{F}_h$ are collected in the set $\mathcal{E}_\sigma$. The volume of a face σ is denoted by $|\sigma|$ and that of an edge e by $|e|$. Finally, we use the notation $\mathbf{x}_K$ to denote the

"center" of the cell $K \in \mathcal{T}_h$. If $\sigma = K|L \in \mathcal{F}_h$ separates the cells K and L, $d_{K,L}$ denotes the Euclidean distance between $\mathbf{x}_K$ and $\mathbf{x}_L$, and $d_{K,\sigma}$ for $\sigma \in \mathcal{F}_K$ denotes the distance from $\mathbf{x}_K$ to σ. Similarly, we let $\mathbf{x}_\sigma$ be the "center" of the face σ and $\mathbf{x}_e$ the "center" of the edge e and denote respectively by $d_{\sigma,\tilde{\sigma}}$ and $d_{\sigma,e}$ the distance between $\mathbf{x}_\sigma$ and $\mathbf{x}_{\tilde{\sigma}}$ for $e = \sigma|\tilde{\sigma} \in \mathcal{E}_{h,i}^{\text{int}}$ and the distance from $\mathbf{x}_\sigma$ to e for $e \in \mathcal{E}_\sigma$.

We assume that the composite mesh $\mathcal{T}_h$ satisfies the following orthogonality condition: for an interface $\sigma = K|L$, the line segment $\mathbf{x}_K\mathbf{x}_L$ is orthogonal to this interface (see [27]). The same condition should be satisfied for an edge $e = \sigma|\tilde{\sigma} \in \mathcal{E}_{h,i}^{\text{int}}$ due to the discretization of the Ventcell operator (see Fig. 4.1).

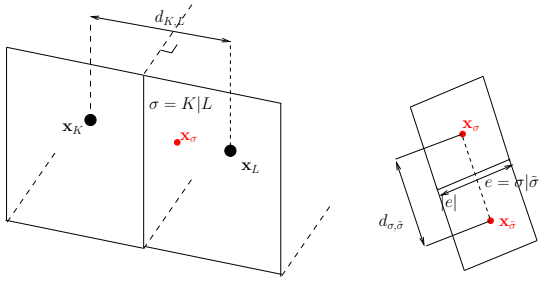

Figure 4.1. Notation for admissible meshes in three space dimensions

4.1.2. *Time discretization*

For an integer $N \geq 0$, let $(\tau^n)_{0 \leq n \leq N}$ denote a sequence of positive real numbers corresponding to the discrete time steps such that $T = \sum_{n=1}^{N} \tau^n$. Let $t^0 = 0$, and $t^n = \sum_{j=1}^{n} \tau^j,\ 1 \leq n \leq N$, be the discrete times. Let $I^n = (t^{n-1}, t^n],\ 1 \leq n \leq N$. For simplicity, we consider only conforming time grids. The analysis remains valid if we use different time steps in the subdomains, as was done in [7] for a linear diffusion problem.

4.1.3. *Notation and discrete function spaces*

We denote by $\mathbb{P}_l(S)$ the space of polynomials on a subdomain $S \subset \Omega$ of total degree less than or equal to l and by

$$\mathbb{P}_l(\mathcal{T}_h) := \{p_h \in L^2(\Omega);\ p_h|_K \in \mathbb{P}_l(K),\ \forall K \in \mathcal{T}_h\},$$

the space of piecewise l-degree polynomials on $\mathcal{T}_h$. We use the notation $\|\cdot\|_K$ for the norm in $L^2(K),\ K \in \mathcal{T}_h$. The corresponding inner product is $(\cdot,\cdot)_K$. We also denote by $(\cdot,\cdot)_\sigma$ the inner product in $L^2(\sigma)$ for $\sigma \in \mathcal{F}_h$. Let $|S|$ be the Lebesgue measure of S, and $|\sigma|$ the $(d-1)$-dimensional Lebesgue measure of $\sigma \in \mathbb{R}^{d-1}$. We define the broken Sobolev space $H^1(\mathcal{T}_h)$ as the space of all functions $v \in L^2(\Omega)$ such that $v|_K \in H^1(K)$, for all $K \in \mathcal{T}_h$. We will use the sign ∇ to denote the elementwise gradient, i.e., the gradient of a function restricted to a mesh element $K \in \mathcal{T}_h$. We define $P_\tau^1(H^1(\mathcal{T}_h))$ and $P_\tau^1(H_0^1(\Omega))$ as the space of continuous and piecewise affine in-time functions $v_{h\tau}$ with values in $H^1(\mathcal{T}_h)$ and in $H_0^1(\Omega)$, respectively. In both these situations, for every time step $1 \leq n \leq N$, we will use the abridged notation $v_h^n := v_{h\tau}(\cdot, t^n)$. By Assumption 2.1, the source function f is piecewise constant in time, i.e., constant on each time interval $I^n,\ 1 \leq n \leq N$. Its value on I^n is denoted by $f^n := f|_{I^n}$.

The domain decomposition method we consider is global in time. Thus, at the space-time interface $\Gamma \times (0,T)$, data should be transferred from one space-time subdomain to the neighboring subdomain. Then, we denote by $P_\tau^0(L^2(\Gamma))$ the space of functions piecewise constant in time and with values in $L^2(\Gamma)$. Let $\mathbf{H}(\text{div}, \Omega)$ be the space of vector-valued functions from $\left[L^2(\Omega)\right]^d$ that admit a weak

divergence in $L^2(\Omega)$. Recall that all functions in $\mathbf{H}(\mathrm{div},\Omega)$ have a continuous normal trace across the interface Γ. As above, $P^0_\tau(\mathbf{H}(\mathrm{div},\Omega))$ is the space of functions piecewise constant in time with values in $\mathbf{H}(\mathrm{div},\Omega)$. We use $\mathbf{RTN}_0(\Omega)$ to denote the lowest-order Raviart–Thomas–Nédélec finite-dimensional subspace of $\mathbf{H}(\mathrm{div},\Omega)$; any $\mathbf{v}_h \in \mathbf{RTN}_0(\Omega)$ takes on each element $K \in \mathcal{T}_h$ the form $[\mathbb{P}_0(K)]^d + \mathbb{P}_0(K)\mathbf{x}$ for the example of simplices.

Finally, given a function v that is double-valued on the interface Γ, the jump and the average of v across a face $\sigma \in \mathcal{F}_h^\Gamma$, $\sigma = K|L$, $K \in \mathcal{T}_{h,1}$, $L \in \mathcal{T}_{h,2}$, are defined as

$$[\![v]\!] = (v_K)\,|_\sigma - (v_L)\,|_\sigma, \qquad \{\!\{v\}\!\} = \frac{(v_K)\,|_\sigma + (v_L)\,|_\sigma}{2}.$$

Here $v_K = v|_K$ is the restriction of v to the element $K \in \mathcal{T}_h$.

4.2. A space-time fully discrete scheme based on finite volumes in space and the backward Euler scheme in time

For the iteration $k \geq 1$ of the OSWR algorithm (3.3)–(3.4), subdomain Ω_i, $i = 1, 2$, and the time steps $0 \leq n \leq N$, let the *discrete saturation* be identified with the vector of unknowns

$$\left((u_K^{k,n})_{K\in\mathcal{T}_{h,i}}, (u_{K,\sigma}^{k,n})_{\sigma\in\mathcal{F}_K\cap\mathcal{F}_h^\Gamma, K\in\mathcal{T}_{h,i}}\right).$$

Note that there are in total two interface unknowns $u_{K,\sigma}^{k,n}$ for each face σ of $\mathcal{F}_h^\Gamma$, in addition to the usual one unknown $u_K^{k,n}$ per mesh element.

We then define the discrete flux $F_{K,\sigma}^{k,n}$ over a face $\sigma \in \mathcal{F}_h \cap \mathcal{F}_K$, $K \in \mathcal{T}_{h,i}$, by

$$F_{K,\sigma}^{k,n} := \begin{cases} \dfrac{\varphi_i(u_K^{k,n}) - \varphi_i(u_L^{k,n})}{d_{K,L}}, & \text{if } \sigma = K|L \in \mathcal{F}_{h,i}^{\mathrm{int}}, \\ \dfrac{\varphi_i(u_K^{k,n}) - \varphi_i(g_i(\mathbf{x}_\sigma))}{d_{K,\sigma}}, & \text{if } \sigma \in \mathcal{F}_K \cap \mathcal{F}_{h,i}^{\mathrm{D}}, \\ \dfrac{\varphi_i(u_K^{k,n}) - \varphi_i(u_{K,\sigma}^{k,n})}{d_{K,\sigma}}, & \text{if } \sigma \in \mathcal{F}_K \cap \mathcal{F}_h^\Gamma, \end{cases} \tag{4.1a}$$

and the discrete $(d-1)$-dimensional flux $\bar{F}_{\sigma,e}^{k,n}$ over an edge $e \in \mathcal{E}_\sigma$, $\sigma \in \mathcal{F}_K \cap \mathcal{F}_h^\Gamma$, $K \in \mathcal{T}_{h,i}$, by

$$\bar{F}_{\sigma,e}^{k,n} := \begin{cases} \dfrac{\Pi_i(u_{K,\sigma}^{k,n}) - \Pi_i(u_{K,\tilde{\sigma}}^{k,n})}{d_{\sigma,\tilde{\sigma}}}, & \text{if } e = \sigma|\tilde{\sigma} \in \mathcal{E}_\sigma \cap \mathcal{E}_{h,i}^{\mathrm{int}}, \\ \dfrac{\Pi_i(u_{K,\sigma}^{k,n}) - \Pi_i(g_i(\mathbf{x}_e))}{d_{\sigma,e}}, & \text{if } e \in \mathcal{E}_\sigma \cap \mathcal{E}_{h,i}^{\mathrm{D}}. \end{cases} \tag{4.1b}$$

We also define the Ventcell term, for $K \in \mathcal{T}_{h,i}$,

$$\left(\Lambda_{K,\Gamma}^{k,n}\right)_\sigma := \alpha_{i,j}|\sigma|\Pi_i(u_{K,\sigma}^{k,n}) + \gamma_{i,j}\sum_{e\in\mathcal{F}_\sigma}|e|\bar{F}_{\sigma,e}^{k,n}, \quad \sigma \in \mathcal{F}_K \cap \mathcal{F}_h^\Gamma, \tag{4.2}$$

and the information from Ω_j, for $L \in \mathcal{T}_{h,j}$, $j = 3 - i$, and $\sigma = K|L \in \mathcal{F}_h^\Gamma$,

$$\Psi_{L,\sigma}^{k-1,n} := F_{L,\sigma}^{k-1,n}|\sigma| + \gamma_{i,j}\frac{\Pi_j(u_{L,\sigma}^{k-1,n}) - \Pi_j(u_{L,\sigma}^{k-1,n-1})}{\tau^n}|\sigma| + \left(\Lambda_{L,\Gamma}^{k-1,n}\right)_\sigma. \tag{4.3}$$

Using (4.1), the approximation of the solution u^k in the OSWR algorithm (3.3)–(3.4) is: at each iteration $k \geq 1$, the initial condition is given by

$$u_K^{k,0} = \frac{1}{|K|}(u_0, 1)_K, \qquad \forall K \in \mathcal{T}_h, \tag{4.4a}$$

and for $n = 1, \ldots, N$, the discrete saturations are given by the following *finite volume scheme*:

$$\frac{u_K^{k,n} - u_K^{k,n-1}}{\tau^n}|K| + \sum_{\sigma \in \mathcal{F}_K} |\sigma| F_{K,\sigma}^{k,n} = (f_i^n, 1)_K \quad \forall K \in \mathcal{T}_{h,i}, \tag{4.4b}$$

$$-F_{K,\sigma}^{k,n}|\sigma| + \gamma_{i,j}\frac{\Pi_i(u_{K,\sigma}^{k,n}) - \Pi_i(u_{K,\sigma}^{k,n-1})}{\tau^n}|\sigma| + \left(\Lambda_{K,\Gamma}^{k,n}\right)_\sigma = \Psi_{L,\sigma}^{k-1,n}, \quad \forall \sigma = K|L \in \mathcal{F}_h^\Gamma. \tag{4.4c}$$

4.3. **Newton linearization**

At *Newton linearization* step $m \geq 1$ the following problem is to be solved:

For $i = 1, 2$, find $\left((u_K^{k,n,m})_{K \in \mathcal{T}_{h,i}}, (u_{K,\sigma}^{k,n,m})_{\sigma \in \mathcal{F}_K \cap \mathcal{F}_h^\Gamma, K \in \mathcal{T}_{h,i}}\right) \in \mathbb{P}_0(\mathcal{T}_{h,i}) \times \mathbb{P}_0(\mathcal{F}_h^\Gamma)$ such that

$$\frac{u_K^{k,n,m} - u_K^{k,n-1}}{\tau^n}|K| + \sum_{\sigma \in \mathcal{F}_K} |\sigma| F_{K,\sigma}^{k,n,m-1} = (f_i^n, 1)_K, \quad \forall K \in \mathcal{T}_{h,i}, \tag{4.5a}$$

$$-|\sigma| F_{K,\sigma}^{k,n,m-1} + \gamma_{i,j}\frac{\Pi_i^{m-1}(u_{K,\sigma}^{k,n,m}) - \Pi_i(u_{K,\sigma}^{k,n-1})}{\tau^n}|\sigma| + \left(\Lambda_{K,\Gamma}^{k,n,m-1}\right)_\sigma = \Psi_{L,\sigma}^{k-1,n}, \quad \forall \sigma = K|L \in \mathcal{F}_h^\Gamma, \tag{4.5b}$$

where $F_{K,\sigma}^{k,n,m-1}$ are the linearized face fluxes and $\Lambda_{K,\Gamma}^{k,n,m-1}$ are the linearized Ventcell terms (affine functions of $u_K^{k,n,m}$ and $u_{K,\sigma}^{k,n,m}$ obtained by linearization around the available $u_K^{k,n,m-1}$ and $u_{K,\sigma}^{k,n,m-1}$, see [1] for details), and the function Π_i is linearized by

$$\Pi_i^{m-1}(u_{K,\sigma}^{k,n,m}) := \Pi_i(u_{K,\sigma}^{k,n,m-1}) + \frac{\partial \Pi_i}{\partial u_{K,\sigma}}(u_{K,\sigma}^{k,n,m-1}) \cdot (u_{K,\sigma}^{k,n,m} - u_{K,\sigma}^{k,n,m-1}).$$

Equations (4.5a)–(4.5b) form a system of *linear algebraic equations* that is solved at each domain decomposition iteration k, time step n, and Newton iteration m, *independently* in *each of the subdomains* Ω_i.

5. **Postprocessing and H^1- and H(div)-conforming reconstructions**

So far, we have described the OSWR domain decomposition algorithm and its finite volume discretization. In the next four sections, we address the important question of assessing the accuracy of the approximate solution, both as a function of the space and time discretization parameters, and as a function of the OSWR and Newton iterations. This is achieved by deriving detailed a posteriori error estimators for each of the possible error components.

At each OSWR iteration $k \geq 1$, time step $0 \leq n \leq N$, and linearization step $m \geq 1$, we dispose of the piecewise constant in space and in time approximation of the saturation given by the values $u_K^{k,n,m}$, $K \in \mathcal{T}_h$, defined in (4.5). In this section, we develop basic tools that will allow us to build the estimators. We extend for this purpose to the present setting the approach of [25, 45, 54, 23] and the references therein and proceed in three steps:

(i) Define a *locally postprocessed saturation* $u_{h\tau}^{k,m}$ that is elementwise more regular than the piecewise constants $u_K^{k,n,m}$, $K \in \mathcal{T}_h$. This is customary in finite volume methods, as an energy-norm-type a posteriori error estimate has no meaning for the piecewise constants. There, however,

holds (recall that we use the notation $u_{h\tau,i}^{k,m} = u_{h\tau}^{k,m}|_{\Omega_i}$)

$$\varphi_i(u_{h\tau,i}^{k,m}) \notin X_{\varphi_i(g_i)},\ i=1,2, \quad \text{and} \quad \Pi_1(u_{h\tau,1}^{k,m}) \neq \Pi_2(u_{h\tau,2}^{k,m}) \text{ on } \Gamma, \tag{5.1}$$

since $u_{h\tau}^{k,m}$ is discontinuous between mesh elements. Thus, $u_{h\tau}^{k,m}$ is a *nonconforming approximation* of the weak solution of Definition 2.2 that has to in particular satisfy properties 3 and 4.

(ii) Define a *saturation reconstruction* $s_{h\tau}^{k,m}$ that is *conforming* in the sense of Definition 2.2, satisfying all

$$s_{h\tau}^{k,m} \in Z, \qquad \varphi_i(s_{h\tau,i}^{k,m}) \in X_{\varphi_i(g_i)},\ i=1,2, \qquad \Pi(s_{h\tau}^{k,m},\cdot) \in X_{\Pi(g,\cdot)}. \tag{5.2}$$

This is a first crucial ingredient of our a posteriori error estimate and plays the role of the potential reconstruction in terms of [25]. It will be constructed cheaply, in an explicit way by local averaging.

(iii) Define an *equilibrated flux reconstruction* $\boldsymbol{\sigma}_{h\tau}^{k,m}$ (in terms of [25]), piecewise constant in-time and $\mathbf{H}(\mathrm{div},\Omega)$-conforming, locally conservative on the mesh $\mathcal{T}_h$:

$$\boldsymbol{\sigma}_h^{k,n,m} := \boldsymbol{\sigma}_{h\tau}^{k,m}|_{I^n} \in \mathbf{RTN}_0(\Omega), \tag{5.3a}$$

$$\left(f^n - \frac{u_K^{k,n,m} - u_K^{k,n-1}}{\tau^n} - \nabla\cdot\boldsymbol{\sigma}_h^{k,n,m}, 1\right)_K = 0, \quad \forall K \in \mathcal{T}_h. \tag{5.3b}$$

This is again constructed cheaply, by solving a coarse problem at each time step followed by some local Neumann problems in bands close to the interface.

5.1. Postprocessed saturation $u_{h\tau}^{k,m}$

Consider an OSWR iteration $k \geq 1$, time step $1 \leq n \leq N$, and a linearization step $m \geq 1$.

Extending [28, 25] to the present nonlinear context, we define the postprocessed approximation $\varphi_{h,i}^{k,n,m} \in \mathbb{P}_2(\mathcal{T}_{h,i})$ such that $\nabla\varphi_{h,i}^{k,n,m} \in \mathbf{RTN}_0(K)$ in each element $K \in \mathcal{T}_{h,i}$, as the solution of

$$(-\nabla\varphi_{h,i}^{k,n,m}|_K\cdot\mathbf{n}_i)|_\sigma = F_{K,\sigma}^{k,n,m-1} \qquad \forall\sigma \in \mathcal{F}_K, \tag{5.4a}$$

$$\frac{(\varphi_i^{-1}(\varphi_{h,i}^{k,n,m}),1)_K}{|K|} = u_K^{k,n,m}. \tag{5.4b}$$

Procedure (5.4) is local in each mesh element and its cost is negligible. From $\varphi_{h,i}^{k,n,m}$, we construct the corresponding continuous, piecewise affine in-time postprocessed saturation by

$$u_{h\tau,i}^{k,m}(\cdot,t_n) = \varphi_i^{-1}(\varphi_{h,i}^{k,n,m}),\ 1 \leq n \leq N. \tag{5.5}$$

Note that $u_{h\tau}^{k,m}$ is nonconforming in the sense of (5.1).

Remark 5.1 (Practice)**.** *In practice, condition* (5.4b) *is typically approximated by the quadrature rule* $\varphi_{h,i}^{k,n,m}(\mathbf{x}_K) = \varphi_i(u_K^{k,n,m})\ \forall K \in \mathcal{T}_{h,i}$*, so that* $\varphi_{h,i}^{k,n,m}$ *becomes readily available. Moreover, the significant estimators in Theorem 6.1 below only involve* $\varphi_{h,i}^{k,n,m}$ *and not* $u_{h\tau,i}^{k,m}$*, which then needs not be constructed in practice.*

5.2. Subdomain H^1-conforming reconstruction $s_{h\tau}^{k,m}$

We define in this section the saturation reconstruction $s_{h\tau}^{k,m}$. It will belong to $H^1(\Omega_i)$, $i = 1, 2$, and satisfy (5.2) (up to numerical quadrature). In contrast to the usual scenario, see [25, 45, 54], we cannot immediately apply the operator $\mathcal{I}_{\rm av}$ that prescribes averages at the Lagrange degrees of freedom to the postprocessed saturation $u_{h\tau}^{k,m}$ constructed in Section 5.1, since $u_{h\tau}^{k,m}$ is generally not a piecewise polynomial and, moreover, it may not be constructed in practice, see Remark 5.1. Instead, we proceed in two steps.

First, from the available $\varphi_{h,i}^{k,n,m} \in \mathbb{P}_2(\mathcal{T}_{h,i})$ defined by (5.4), $k \geq 1$, $1 \leq n \leq N$, $m \geq 1$, we define a piecewise polynomial that is continuous in each subdomain Ω_i by

$$\mathcal{I}_{\rm av}(\varphi_{h,i}^{k,n,m}).$$

Here $\mathcal{I}_{\rm av} : \mathbb{P}_2(\mathcal{T}_{h,i}) \to \mathbb{P}_2(\mathcal{T}_{h,i}) \cap H^1(\Omega_i)$ is the averaging operator given by

$$\mathcal{I}_{\rm av}(\phi_h)(\mathbf{x}) = \frac{1}{|\mathcal{T}_\mathbf{x}|} \sum_{K \in \mathcal{T}_\mathbf{x}} \phi_h|_K(\mathbf{x}),$$

with $\mathcal{T}_\mathbf{x}$ the set of all the elements of $\mathcal{T}_{h,i}$ sharing the Lagrange degree of freedom $\mathbf{x}$, located in the interior of Ω_i or at the interface Γ. Second, we consider $\varphi_i^{-1}(\mathcal{I}_{\rm av}(\varphi_{h,i}^{k,n,m})(\mathbf{x}))$ at the Lagrange degrees of freedom $\mathbf{x}$ to define $s_h^{k,n,m}$; we modify it at the interface Γ, on the boundaries $\Gamma_i^{\rm D}$, and in the element interiors to satisfy

$$\Pi_1(s_h^{k,n,m}|_{\Omega_1}) = \Pi_2(s_h^{k,n,m}|_{\Omega_2}) \text{ on } \Gamma, \tag{5.6a}$$

$$s_h^{k,n,m}|_{\Gamma_i^{\rm D}} = g_i \text{ on } \Gamma_i^{\rm D},\ i = 1, 2, \tag{5.6b}$$

$$\frac{1}{|K|}(s_h^{k,n,m}, 1)_K = u_K^{k,n,m}, \quad \forall K \in \mathcal{T}_h. \tag{5.6c}$$

Finally, the continuous piecewise affine in-time function $s_{h\tau}^{k,m}$ is prescribed by

$$s_{h\tau}^{k,m}(\cdot, t_n) = s_h^{k,n,m}, \qquad 1 \leq n \leq N. \tag{5.7}$$

Remark 5.2 (Practice)**.** *In practice, condition* (5.6a) *will again only be satisfied in the sense of quadrature. The last condition* (5.6c) *is easy to satisfy using the bubble functions following* [25, Section 3.2.2]*, again up to a quadrature error.*

5.3. Equilibrated flux reconstruction $\boldsymbol{\sigma}_{h\tau}^{k,m}$

Because of the domain decomposition formulation with Robin or Ventcell transmission conditions, the finite volume fluxes $F_{K,\sigma}^{k,n}$ of (4.1a) (or their linearizations $F_{K,\sigma}^{k,n,m-1}$) do not match across the two sides of the interface Γ. Consequently, $-\nabla\varphi_h^{k,n,m}$ is not $\mathbf{H}(\mathrm{div}, \Omega)$-conforming (it does not lie in the space $\mathbf{RTN}_0(\Omega)$), and cannot be used as a flux reconstruction in the sense of (5.3). To obtain $\boldsymbol{\sigma}_{h\tau}^{k,m}$, the procedure used in the linear case in [6, 7] can be employed here. The details are given in Appendix A.

6. A posteriori error estimate

Relying on the developments of the previous sections, we derive here an a posteriori error estimate that bounds an energy error between the postprocessed saturation $u_{h\tau}^{k,m}$ defined in Section 5.1 and the weak solution u of Definition 2.2 by a guaranteed and fully computable upper bound, and this at *each OSWR iteration* $k \geq 1$ and at *each linearization step* $m \geq 1$.

For all times $t \in (0,T)$, let

$$Q_{t,i} := L^2(0,t;L^2(\Omega_i)), \qquad X_t := L^2(0,t;H_0^1(\Omega)), \qquad X_t' := L^2(0,t;H^{-1}(\Omega)).$$

Because of the assumptions on the weak solution u in Definition 2.2 and since, by (5.5), $\varphi_i(u_{h\tau,i}^{k,m}) \in L^2(0,T;L^2(\Omega_i))$ for the postprocessed saturation $u_{h\tau}^{k,m}$ defined in Section 5.1, $u_{h\tau}^{k,m} \in X'$, and $u_{h\tau}^{k,m}(\cdot,T) \in H^{-1}(\Omega)$, we can define an energy-type error following [23] as

$$\begin{aligned}
&\|u - u_{h\tau}^{k,m}\|_\sharp^2 \\
&:= \sum_{i=1}^2 \|\varphi_i(u_i) - \varphi_i(u_{h\tau,i}^{k,m})\|_{Q_{T,i}}^2 + \frac{L_\varphi}{2}\|u - u_{h\tau}^{k,m}\|_{X'}^2 + \frac{L_\varphi}{2}\|(u - u_{h\tau}^{k,m})(\cdot,T)\|_{H^{-1}(\Omega)}^2 \\
&\quad + 2\sum_{i=1}^2 \int_0^T \left(\|\varphi_i(u_i) - \varphi_i(u_{h\tau,i}^{k,m})\|_{Q_{t,i}}^2 + \int_0^t \|\varphi_i(u_i) - \varphi_i(u_{h\tau,i}^{k,m})\|_{Q_{s,i}}^2 e^{t-s}\mathrm{d}s \right)\mathrm{d}t,
\end{aligned} \tag{6.1}$$

where we recall that L_φ is the maximal Lipschitz constant of the functions φ_i defined by (2.7).

The saturation reconstruction $s_{h\tau}^{k,m}$ defined in Section 5.2 is conforming in the sense of Definition 2.2 in that it satisfies (5.2). Consequently, it can be plugged into the weak form (2.12) to yield the residual

$$\langle \mathcal{R}(s_{h\tau}^{k,m}), \psi\rangle_{X',X} := \int_0^T \Big\{ (f,\psi) - \langle \partial_t s_{h\tau}^{k,m}, \psi\rangle_{H^{-1}(\Omega),H_0^1(\Omega)} - \sum_{i=1}^2 (\nabla\varphi_i(s_{h\tau,i}^{k,m}), \nabla\psi)_{\Omega_i} \Big\}(\theta)\mathrm{d}\theta. \tag{6.2}$$

The dual norm of the residual $\mathcal{R}(s_{h\tau}^{k,m})$ on X' is then given by

$$\|\mathcal{R}(s_{h\tau}^{k,m})\|_{X'} := \sup_{\psi\in X,\, \|\psi\|_X = 1} \langle \mathcal{R}(s_{h\tau}^{k,m}), \psi\rangle_{X',X} \tag{6.3}$$

and expresses by how much $s_{h\tau}^{k,m}$ fails to satisfy (2.12); we will also use similar notation for X_t', where T is replaced by t. We finally define the weaker error

$$\begin{aligned}
\|u - s_{h\tau}^{k,m}\|_\flat := \sqrt{\frac{L_\varphi}{2}} \Bigg\{ &(2e^T - 1)\|u_0 - s_{h\tau}^{k,m}(\cdot,0)\|_{H^{-1}(\Omega)}^2 + \|\mathcal{R}(s_{h\tau}^{k,m})\|_{X'}^2 \\
&+ 2\int_0^T \Big(\|\mathcal{R}(s_{h\tau}^{k,m})\|_{X_t'}^2 + \int_0^t \|\mathcal{R}(s_{h\tau}^{k,m})\|_{X_s'}^2 e^{t-s}\mathrm{d}s \Big)\mathrm{d}t \Bigg\}^{\frac{1}{2}}.
\end{aligned} \tag{6.4}$$

For the iteration $k \geq 1$ of the OSWR algorithm, for a linearization step $m \geq 1$, and for a time step $1 \leq n \leq N$, we define the *initial condition*, *residual*, and *discretization* estimators respectively by:

$$\eta_{\mathrm{IC}}^{k,m} := \|u_0 - s_{h\tau}^{k,m}(\cdot,0)\|_{H^{-1}(\Omega)}, \tag{6.5a}$$

$$\eta_{\mathrm{R},K}^{k,n,m} := C_{\mathrm{P},K} h_K \|f^n - \partial_t s_{h\tau}^{k,m} - \nabla\cdot\boldsymbol{\sigma}_h^{k,n,m}\|_K, \quad K \in \mathcal{T}_h, \tag{6.5b}$$

$$\eta_{\mathrm{disc},K,i}^{k,n,m}(t) := \|\boldsymbol{\sigma}_h^{k,n,m} + \nabla\varphi_i(s_{h\tau}^{k,m}(\cdot,t))\|_K, \quad K \in \mathcal{T}_{h,i},\ t \in I^n, \quad i = 1,2, \tag{6.5c}$$

where, in (6.5b), $C_{\mathrm{P},K}$ is the constant in the Poincaré inequality:

$$\|q - q_K\| \leq C_{\mathrm{P},K} h_K \|\nabla q\|_K \quad \forall q \in H^1(K),$$

with q_K the mean value of the function q on the element K and $C_{\mathrm{P},K} = 1/\pi$ whenever K is convex. Then the estimators $\eta^{k,n,m}$ and $\eta^{k,m}$ are respectively defined by

$$\eta^{k,n,m} := \left\{ \int_{I^n} \sum_{i=1}^{2} \sum_{K \in \mathcal{T}_{h,i}} \left(\eta_{\mathrm{R},K}^{k,n,m} + \eta_{\mathrm{disc},K,i}^{k,n,m}(t) \right)^2 \mathrm{d}t \right\}^{\frac{1}{2}}, \quad 1 \le n \le N, \tag{6.5d}$$

$$\begin{aligned} \eta^{k,m} := \sqrt{\frac{L_\varphi}{2}} \Bigg\{ & (2e^T - 1)(\eta_{\mathrm{IC}}^{k,m})^2 + \sum_{n=1}^{N} \left(\eta^{k,n,m} \right)^2 \\ & + 2 \sum_{n=1}^{N} \tau^n \sum_{l=1}^{n} (\eta^{k,l,m})^2 + 2 \sum_{n=1}^{N} \sum_{l=1}^{n} \left(\int_{I^n} \int_{I^l} e^{t-s} \mathrm{d}s\mathrm{d}t \right) \left(\sum_{q=1}^{l} \left(\eta^{k,q,m} \right)^2 \right) \Bigg\}^{\frac{1}{2}}. \end{aligned} \tag{6.5e}$$

Our main result is stated in the following theorem:

Theorem 6.1 (A posteriori error estimate)**.** *Let u be the weak solution of the multidomain problem* (2.9)–(2.10) *in the sense of Definition 2.2. Consider the Ventcell–OSWR algorithm* (3.3)–(3.4) *at iteration $k \ge 1$, the finite volume discretization of Section 4.2 on space and time meshes indexed by h and τ, and the Newton linearization of Section 4.3 on step $m \ge 1$. Let $u_{h\tau}^{k,m}$ be the postprocessed saturation of Section 5.1, $s_{h\tau}^{k,m}$ the saturation reconstruction of Section 5.2, and $\boldsymbol{\sigma}_{h\tau}^{k,m}$ the equilibrated flux reconstruction of Section 5.3. Then*

$$\|u - s_{h\tau}^{k,m}\|_\flat \le \eta^{k,m}. \tag{6.6}$$

Moreover, if

$$\bar{\varphi} \in X, \qquad \text{where} \qquad \bar{\varphi}|_{\Omega_i} := \varphi_i(u_i) - \varphi_i(s_{h\tau,i}^{k,m}), \quad i = 1, 2, \tag{6.7}$$

then

$$\|u - u_{h\tau}^{k,m}\|_\sharp \le \eta^{k,m} + \|u_{h\tau}^{k,m} - s_{h\tau}^{k,m}\|_\sharp. \tag{6.8}$$

Proof. We have defined $s_{h\tau}^{k,m}$ so that $\varphi_i(s_{h\tau,i}^{k,m}) \in X_{\varphi_i(g_i)}$, $\Pi(s_{h\tau}^{k,m}, \cdot) \in X_{\Pi(g,\cdot)}$, and

$$(f^n - \partial_t s_{h\tau}^{k,m}|_{I^n} - \nabla{\cdot}\boldsymbol{\sigma}_h^{k,n,m}, 1)_K = 0 \qquad \forall K \in \mathcal{T}_h,\ 1 \le n \le N. \tag{6.9}$$

Indeed, (6.9) follows from the requirement (5.6c) which implies

$$(\partial_t s_{h\tau}^{k,m}|_{I^n}, 1)_K = \left(\frac{s_h^{k,n,m} - s_h^{k,n-1}}{\tau^n}, 1 \right)_K = \left(\frac{u_K^{k,n,m} - u_K^{k,n-1}}{\tau^n}, 1 \right)_K$$

together with (5.3b). Thus, adding and subtracting $(\boldsymbol{\sigma}_{h\tau}^{k,m}, \nabla\psi)$ in (6.2) and using Green's theorem and the fact that $\partial_t s_{h\tau}^{k,m} \in L^2(0,T;L^2(\Omega))$, we infer

$$\begin{aligned} & \langle \mathcal{R}(s_{h\tau}^{k,m}), \psi \rangle_{X',X} \\ & = \sum_{n=1}^{N} \int_{I^n} \Big\{ (f - \partial_t s_{h\tau}^{k,m} - \nabla{\cdot}\boldsymbol{\sigma}_h^{k,n,m}, \psi) - \sum_{i=1}^{2} (\nabla\varphi_i(s_{h\tau,i}^{k,m}) + \boldsymbol{\sigma}_h^{k,n,m}, \nabla\psi)_{\Omega_i} \Big\}(\theta)\mathrm{d}\theta. \end{aligned}$$

From (6.3) and using (6.9), it then immediately follows that

$$\|\mathcal{R}(s_{h\tau}^{k,m})\|_{X'}^2 \le \sum_{n=1}^{N} \left(\eta^{k,n,m} \right)^2.$$

Proceeding as in [23, Theorem 5.3], we then promptly arrive at (6.6). Next, it follows by inspection of the proof of [23, Theorem 5.2] that, under assumption (6.7), we have

$$\|u - s_{h\tau}^{k,m}\|_\sharp \le \|u - s_{h\tau}^{k,m}\|_\flat. \tag{6.10}$$

Thus (6.8) follows by the triangle inequality

$$\|u - u_{h\tau}^{k,m}\|_\sharp \le \|u - s_{h\tau}^{k,m}\|_\sharp + \|u_{h\tau}^{k,m} - s_{h\tau}^{k,m}\|_\sharp.$$

■

Remark 6.2 (Condition (6.7))**.** *Condition* (6.7) *seems unfortunately necessary to apply* [23, Theorem 5.2] *so as to obtain* (6.10) *and consequently the a posteriori estimate* (6.8)*. It is indeed rather restrictive for the complete problem* (2.9)–(2.10)*. It is, though, in particular satisfied when the global mobilities of the gas* λ_i *are constants in the respective subdomains* Ω_i *and* $\pi_1(0) = \pi_2(0)$*. In this case, we get an estimate in the norm* $\|\cdot\|_\sharp$ *defined by* (6.1) *for the present nonlinear degenerate parabolic problem, where the transmission conditions are nonlinear and indeed discontinuous, since* $\overline{\pi}_1(u_1) = \overline{\pi}_2(u_2)$ *but* $u_1 \neq u_2$ *in general at the interface* Γ*. In general, when condition* (6.7) *is not satisfied, we only control the dual residual norm* $\|\cdot\|_\flat$ *defined by* (6.4)*.*

Remark 6.3 (A posteriori estimate of the saturation and capillary pressure errors)**.** *Applying* (2.8)*, the above estimators bound also the saturation and the capillary pressure errors. More precisely, the estimates still hold if we replace the functions* φ_i *by the functions* Π_i *in* (6.1)*.*

7. Distinguishing the space, time, linearization, and the DD errors

In this section, we distinguish the different error components, proceeding as in [7, 20, 23, 26] and the references therein. The aim is in particular to separate the domain decomposition error from the estimated space, time, and linearization errors.

For the iteration $k \geq 1$ of the OSWR algorithm, for all time steps $1 \leq n \leq N$, a linearization step $m \geq 1$, and both subdomains Ω_i, $i = 1, 2$, we define a vector-valued function $\boldsymbol{\ell}_{h,i}^{k,n,m} \in \mathbf{RTN}(\Omega_i)$ that approximates the available flux used in the Newton iterations in Section 4.3, i.e.,

$$(\boldsymbol{\ell}_{h,i}^{k,n,m} \cdot \mathbf{n}_i)|_\sigma = F_{K,\sigma}^{k,n,m} \qquad \forall \sigma \in \mathcal{F}_K,\, \forall K \in \mathcal{T}_{h,i}, \tag{7.1}$$

where the fluxes $F_{K,\sigma}^{k,n,m}$ are obtained by plugging the available $u_K^{k,n,m}$ to the nonlinear flux expression (4.1a). The vector function $\boldsymbol{\ell}_{h,i}^{k,n,m}$ is called the linearized flux. It tends to $-\nabla\varphi_{h,i}^{k,n,m}$ defined in (5.4a) at convergence of the Newton algorithm. For all $K \in \mathcal{T}_{h,i}$, we then define the local *spatial*, *temporal*, *domain decomposition*, and *linearization* estimators by:

$$\eta_{\mathrm{sp},K,i}^{k,n,m} := \eta_{\mathrm{R},K}^{k,n,m} + \|\nabla\varphi_i(s_{h\tau}^{k,m}(\cdot,t_n)) + \boldsymbol{\ell}_{h,i}^{k,n,m}\|_K, \tag{7.2a}$$

$$\eta_{\mathrm{tm},K,i}^{k,n,m}(t) := \|\nabla(\varphi_i(s_{h\tau}^{k,m}(\cdot,t)) - \varphi_i(s_{h\tau}^{k,m}(\cdot,t_n)))\|_K, \tag{7.2b}$$

$$\eta_{\mathrm{dd},K,i}^{k,n,m} := \|\nabla\varphi_{h,i}^{k,n,m} + \boldsymbol{\sigma}_h^{k,n,m}\|_K, \tag{7.2c}$$

$$\eta_{\mathrm{lin},K,i}^{k,n,m} := \|\nabla\varphi_{h,i}^{k,n,m} + \boldsymbol{\ell}_{h,i}^{k,n,m}\|_K. \tag{7.2d}$$

Note that (7.2c) and (7.2d) only work with lowest-order Raviart–Thomas–Nédélec polynomials, so that they can be evaluated without numerical quadrature error and fast. Set, like in (6.5d), for $\mathrm{a} = \mathrm{sp}, \mathrm{tm}, \mathrm{dd}, \mathrm{lin}$,

$$\big(\eta_{\mathrm{a},i}^{k,n,m}\big)^2 := \int_{I^n} \sum_{K\in\mathcal{T}_{h,i}} \big(\eta_{\mathrm{a},K,i}^{k,n,m}\big)^2 \mathrm{d}t \quad \text{and} \quad \big(\eta_{\mathrm{a}}^{k,n,m}\big)^2 := \sum_{i=1}^{2} \big(\eta_{\mathrm{a},i}^{k,n,m}\big)^2, \tag{7.3}$$

and note that except for $\mathrm{a} = \mathrm{tm}$, $\big(\eta_{\mathrm{a},i}^{k,n,m}\big)^2 = \tau^n \sum_{K\in\mathcal{T}_{h,i}} \big(\eta_{\mathrm{a},K,i}^{k,n,m}\big)^2$; for $\mathrm{a} = \mathrm{tm}$, the dependence of the estimators on time is left implicit. The global versions, like in (6.5e) but without the initial condition,

are

$$\begin{aligned}\eta_{\mathrm{a}}^{k,m} :=& \sqrt{\frac{L_\varphi}{2}}\Bigg(\Bigg\{\sum_{n=1}^{N}\Big(\eta_{\mathrm{a}}^{k,n,m}\Big)^2\Bigg\}^{\frac{1}{2}} + \sqrt{2}\Bigg\{\sum_{n=1}^{N}\tau^n\sum_{l=1}^{n}\Big(\eta_{\mathrm{a}}^{k,l,m}\Big)^2\Bigg\}^{\frac{1}{2}} \\ &+ \sqrt{2}\Bigg\{\sum_{n=1}^{N}\sum_{l=1}^{n}\Big(\int_{I^n}\int_{I^l} e^{t-s}\mathrm{d}s\mathrm{d}t\Big)\sum_{q=1}^{l}\Big(\eta_{\mathrm{a}}^{k,q,m}\Big)^2\Bigg\}^{\frac{1}{2}}\Bigg) + \delta_{\mathrm{a}}\|u_{h\tau}^{k,m} - s_{h\tau}^{k,m}\|_\sharp,\end{aligned} \tag{7.4}$$

where $\delta_{\mathrm{a}} = 0$ for $\mathrm{a} = \mathrm{tm}, \mathrm{dd}, \mathrm{lin}$ and δ_{sp} will take the values 0 or 1, depending on the norm in which the error is measured. Then using estimates (6.8) and (6.6) together with the triangle inequality gives:

Corollary 7.1 (A posteriori error estimate distinguishing error components)**.** *Let the assumptions of Theorem 6.1 be satisfied. Let the linearized flux $\boldsymbol{\ell}_h^{k,n,m}$ be given by* (7.1) *and the estimators by* (6.5a) *and* (7.2)–(7.4)*. Then, with $\delta_{\mathrm{sp}} = 0$,*

$$\|u - s_{h\tau}^{k,m}\|_\flat \le \sqrt{\frac{L_\varphi}{2}}\sqrt{2e^T - 1}\eta_{\mathrm{IC}}^{k,m} + \eta_{\mathrm{sp}}^{k,m} + \eta_{\mathrm{tm}}^{k,m} + \eta_{\mathrm{dd}}^{k,m} + \eta_{\mathrm{lin}}^{k,m},$$

and, under condition (6.7) *and with $\delta_{\mathrm{sp}} = 1$,*

$$\|u - u_{h\tau}^{k,m}\|_\sharp \le \sqrt{\frac{L_\varphi}{2}}\sqrt{2e^T - 1}\eta_{\mathrm{IC}}^{k,m} + \eta_{\mathrm{sp}}^{k,m} + \eta_{\mathrm{tm}}^{k,m} + \eta_{\mathrm{dd}}^{k,m} + \eta_{\mathrm{lin}}^{k,m}.$$

Remark 7.2 (Error components distinction)**.** *The distinction in Corollary 7.1 is merely heuristic, as we do not currently have a proof that our estimates on the individual error components are reliable and efficient bounds on the corresponding error components, i.e., that they represent, up to a constant, their upper and lower bounds. This seems currently out of reach for the present highly nonlinear unsteady problem. The numerical experiments in Section 9 below, though, suggest that $\eta_{\mathrm{dd}}^{k,m}$ is indeed an upper bound on the domain discretization error (cf. Figure 9.3, right), and each component estimate is essentially only sensitive to the corresponding error component (for example, in Figure 9.3, right, essentially only $\eta_{\mathrm{dd}}^{k,m}$ evolves during the DD iterations, whereas in Figure 9.6, essentially only $\eta_{\mathrm{lin}}^{k,m}$ evolves during the linearization iterations). Finer estimates with reliable and efficient separate bounds for the space discretization and linear algebra error components were recently obtained in a simpler setting of a model steady linear problem in* [43, 44]*.*

8. Stopping criteria and optimal balancing of the different error components

We provide here stopping criteria for the OSWR algorithm and the nonlinear solver for the subdomain problems as in [7, 20, 23, 26] and the references therein. The goal is to efficiently use the computer resources while saving many unnecessary iterations and to equilibrate all error components.

Let two real parameters δ_{lin} and δ_{dd} be given in $(0, 1)$. The stopping criteria for the linearization step (inner loop in m) in each subdomain i, at each time step n, and each OSWR iteration k is chosen as, employing the estimates (7.3),

$$\eta_{\mathrm{lin},i}^{k,n,m} \le \delta_{\mathrm{lin}} \max\Big\{\eta_{\mathrm{sp},i}^{k,n,m}, \eta_{\mathrm{tm},i}^{k,n,m}, \eta_{\mathrm{dd},i}^{k,n,m}\Big\}, \quad i = 1, 2. \tag{8.1}$$

Similarly, the stopping criteria for the OSWR algorithm (outer loop in k) is set as, employing the estimates (7.4),

$$\eta_{\mathrm{dd}}^{k,m} \le \delta_{\mathrm{dd}} \max\Big\{\eta_{\mathrm{sp}}^{k,m}, \eta_{\mathrm{tm}}^{k,m}\Big\}. \tag{8.2}$$

The first criterion (8.1) stipulates that there is no need to continue with the linearization iterations if the overall error is dominated by one of the other components. That of the second criterion (8.2)

decides that we stop the OSWR algorithm if the domain decomposition error is dominated by one of the other components. The entire procedure of the approach is then described by the following adaptive algorithm:

Algorithm 1 Complete solution algorithm with adaptive stopping criteria

Require: T, u_0, Ω_i, π_i, λ_i, g_i, and f_i, $i = 1, 2$.
Ensure: The saturations $u_{h\tau}^{k,m}$.

$k := 0$
repeat
  $k := k + 1$
  for i=1,2 **do**
    $j := 3 - i$; $n := 0$
    while $t^n \leq T$ **do**
      $n := n + 1$; $m := 0$
      repeat
        $m := m + 1$
        $u_{h,i}^{k,n,m} := \Upsilon_i(u_{h,i}^{k,n,m-1}, \Psi_j^{k-1,n}, f_i^n, u_{h,i}^{k,n-1})$ by solving (4.5)
        Compute $\eta_{\mathrm{sp},i}^{k,n,m}$, $\eta_{\mathrm{tm},i}^{k,n,m}$, $\eta_{\mathrm{dd},i}^{k,n,m}$, and $\eta_{\mathrm{lin},i}^{k,n,m}$
      until $\eta_{\mathrm{lin},i}^{k,n,m} \leq \delta_{\mathrm{lin}} \max\left\{\eta_{\mathrm{sp},i}^{k,n,m}, \eta_{\mathrm{tm},i}^{k,n,m}, \eta_{\mathrm{dd},i}^{k,n,m}\right\}$
      $u_{h,i}^{k,n} := u_{h,i}^{k,n,m}$
      $\Psi_i^{k-1,n} := \{\Psi_{L,\sigma}^{k-1,n}\}_{\sigma=K|L, K\in\mathcal{T}_{h,i}, L\in\mathcal{T}_{h,j}}$ by (4.3)
    end while
  end for
  Compute $\eta_{\mathrm{sp}}^{k,m}$, $\eta_{\mathrm{tm}}^{k,m}$, $\eta_{\mathrm{dd}}^{k,m}$
until $\eta_{\mathrm{dd}}^{k,m} \leq \delta_{\mathrm{dd}} \max\left\{\eta_{\mathrm{sp}}^{k,m}, \eta_{\mathrm{tm}}^{k,m}\right\}$

Remark 8.1 (Space and time adaptivity)**.** *The above local-in-time estimators are calculated on each element of the mesh and on each time step, and could also be used as indicators in order to refine adaptively the time steps τ^n and/or the space meshes $\mathcal{T}_{h,i}$, see* [20, 23, 54] *and the references therein.*

9. Numerical experiments

In this section we illustrate the efficiency of our theoretical results on numerical experiments.

We have chosen three examples designed to show how the method behaves in various physical and geometrical situations.

- The first example is a simple academic situation (taken from [24]), which already contains the main difficulty, i.e., a discontinuous capillary pressure function. It is chosen to demonstrate the features of the method.
- The second example (from [34]) models the infiltration of a dense non-aqueous phase liquid (DNAPL) in a low-capillarity lens, and involves a geometrically more complex interface that acts as a "capillarity trap".
- In the last example shown (taken from [5]), the flow is tangential to the interface, which may render the application of a DD method more delicate. Furthermore, the capillary pressure function is of a form widely used for two-phase flow simulations (van Genuchten model).

9.1. **Example 1: two rock types with a straight interface**

In a three-dimensional extension of an example from [24], take $\Omega = (0,1)^3$ and $T = 15$. The subdomains are $\Omega_1 = \{0 < x < 1/2\}$ and $\Omega_2 = \{1/2 < x < 1\}$, with $\Gamma = \{x = 1/2\}$. The capillary pressure functions and the global mobilities are given respectively by

$$\pi_1(u) = 5u^2, \qquad \pi_2(u) = 5u^2 + 1, \qquad \lambda_i(u) = u(1-u),\ i \in \{1,2\}. \tag{9.1}$$

We impose Dirichlet conditions on two subsets of the boundary $\partial\Omega$. The saturation is set equal to 0.9 on $\Gamma_{\mathrm{D,in}} = \{(x,y,z) \in \partial\Omega \mid x = 0 \text{ and } 0.4 \le y \le 0.6\}$. On the outflow boundary $\Gamma_{\mathrm{out}} = \{(x,y,z) \in \partial\Omega \mid x = 1\}$, the saturation at time t^{n+1} is set equal to that inside the closest cell at time t^n (see [2]). We assume homogeneous Neumann boundary conditions on the remaining part of the boundary. The initial condition is taken to be zero everywhere, which satisfies (2.6a) and consequently (2.10a) at the interface between the rocks. We take $f = 0$ in Ω_1 and Ω_2. The gas has to go through subdomain Ω_1 before entering subdomain Ω_2. Note that the gas cannot enter the subdomain Ω_2 as long as the capillary pressure $\pi_1(u_1)$ remains lower than the entry pressure $\pi_1(u_1^*)$, with $u_1^* = \dfrac{1}{\sqrt{5}}$, which is physically the phenomenon of capillary trapping that model (2.2) describes and which is mathematically due to the degenerate (vanishing) diffusion: indeed, if diffusion was non-vanishing, the gas saturation would be non-zero in the subdomain Ω_2 from the very beginning (in contrast to the left part of Figure 9.2) and not only after the barrier brake (as in the right part of Figure 9.2).

For the spatial discretization we use uniform meshes in the subdomains, consisting of rectangular parallelepipeds matching on the interface Γ. The implementation is based on the MATLAB Reservoir Simulation Toolbox [40], and makes use of its automatic differentiation feature to compute the Jacobian matrices for solving the nonlinear subdomain problems by the Newton method. The optimized (Robin or Ventcell) parameters are computed by numerically minimizing the continuous convergence factor corresponding to a linearized version of the problem (see Remark 3.1 and [4] for details).

In the rest of this section, we denote the method defined by using the OSWR method with Robin transmission conditions by Robin–OSWR, while the method using full Ventcell transmission conditions will be denoted by Ventcell–OSWR. When appropriate, we qualify the Robin conditions as one-sided ($\alpha_{12} = \alpha_{21}$) or two-sided ($\alpha_{12} \neq \alpha_{21}$) in the more general case.

9.1.1. *The performance of the OSWR method with adaptive stopping criteria*

We first consider the OSWR algorithm with one-sided Robin transmission conditions in (3.2), i.e. $\gamma_{12} = \gamma_{21} = 0$ and $\alpha = \alpha_{1,2} = \alpha_{2,1}$. Two snapshots of the saturation are shown in Fig. 9.1, together with two snapshots of the capillary pressure in Fig. 9.2. As expected, both the saturation of the gas in Ω_1 and the capillary pressure increase until the capillary pressure reaches the entry pressure. It can be seen that the capillary pressure field becomes continuous when the entry pressure is reached; then Ω_2 is infiltrated by the gas, but the saturation remains discontinuous across the interface and some quantity of gas remains trapped under the rock discontinuity.

Next we assess the performance of the optimized parameter α of our Robin–OSWR algorithm of Section 3, see Remark 3.1. Fig. 9.3 (left) shows the domain decomposition estimator $\eta_{\mathrm{dd}}^{k,m}$ (defined in (7.2)–(7.4)) after 25 OSWR iterations as a function of α. The estimator behaves very similarly to what is usually observed for the DD error (see, e.g., [29]). Moreover, the optimized parameter (marked by a square) is close to the value numerically optimal with respect to the estimator $\eta_{\mathrm{dd}}^{k,m}$. This result points the way to the possibility of finding the optimal Robin parameter by minimizing the DD estimator $\eta_{\mathrm{dd}}^{k,m}$. It also confirms the ability of the DD estimator to separate the domain decomposition error from the other components of the total error.

We now analyze the performance of the adaptive stopping criteria (8.2) described in Section 8. In particular, we compare them with the common approach in which the OSWR algorithm is continued

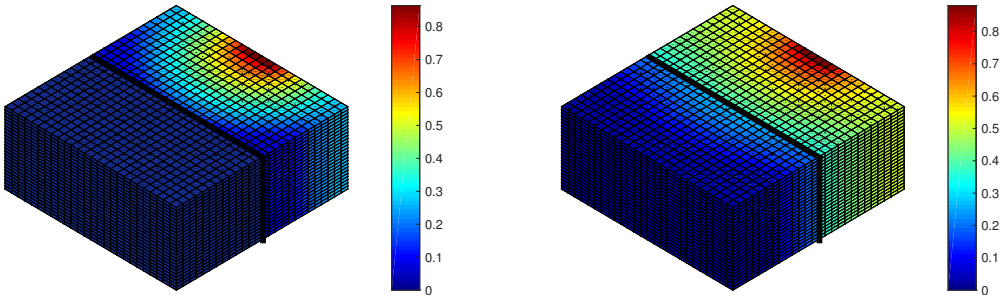

FIGURE 9.1. Example 1: Robin interface conditions, saturation $u(t)$ for $t = 6.6$ and $t = 15$

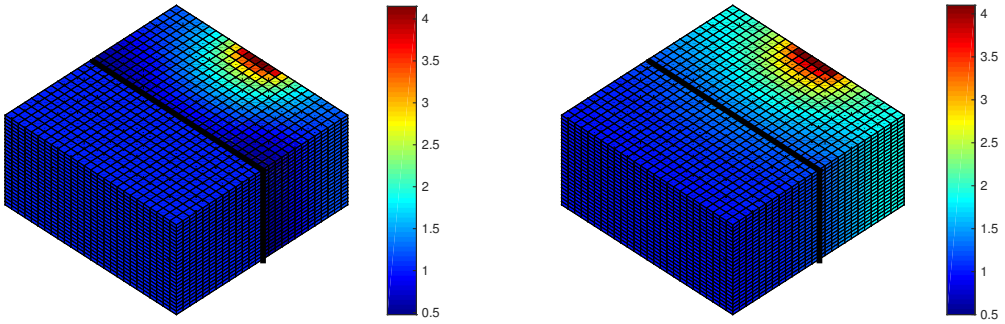

FIGURE 9.2. Example 1: Robin interface conditions, capillary pressure $\pi(u(t), \cdot)$ for $t = 6.6$ and $t = 15$

until the relative Robin residual in L^2-norm on the space-time interface $\Gamma \times (0, T)$ becomes smaller than a threshold taken as 10^{-6}, i.e.,

$$\mathrm{err}_{\mathrm{OSWR}}^{k} := \left(\frac{\sum_{i=1}^{2} \sum_{n=1}^{N} \|\Psi_i^{k,n} - \Psi_i^{k-1,n}\|_{L^2(\Gamma)}^2}{\sum_{i=1}^{2} \sum_{n=1}^{N} \|\Psi_i^{k-1,n}\|_{L^2(\Gamma)}^2} \right)^{\frac{1}{2}} \leq 10^{-6}. \tag{9.2}$$

The Newton iterations are stopped when the residuals in both subdomains Ω_i satisfy

$$\mathrm{err}_{\mathrm{lin},i}^{k,n,m} := \frac{\|\varphi_i(u_{h,i}^{k,n,m}) - \varphi_i(u_{h,i}^{k,n,m-1})\|_{\infty,\Omega_i}}{\|\varphi_i(u_{h,i}^{k,n,m-1})\|_{\infty,\Omega_i}} \leq 10^{-8}. \tag{9.3}$$

In Fig. 9.3 (right), we plot the different estimators as functions of the OSWR iterations. The adaptive stopping criterion (8.2) needs only 10 iterations, while the classical stopping criterion (9.2) requires 21 iterations.

Fig. 9.3 (right) also shows the evolution of the DD error $\|u_{h\tau}^{\infty,m} - u_{h\tau}^{k,m}\|_\sharp$, approximated by

$$\begin{aligned} &\sum_{i=1}^{2} \|\varphi_i(u_{h\tau,i}^{\infty,m}) - \varphi_i(u_{h\tau,i}^{k,m})\|_{Q_{T,i}}^2 \\ &\quad + 2 \sum_{i=1}^{2} \int_0^T \left(\|\varphi_i(u_{h\tau,i}^{\infty,m}) - \varphi_i(u_{h\tau,i}^{k,m})\|_{Q_{t,i}}^2 + \int_0^t \|\varphi_i(u_{h\tau,i}^{\infty,m}) - \varphi_i(u_{h\tau,i}^{k,m})\|_{Q_{s,i}}^2 e^{t-s} \mathrm{d}s \right) \mathrm{d}t, \end{aligned}$$

in brown, where $u_{h\tau,i}^{\infty,m}$ is the postprocessing of the converged DD saturation (computed with a tolerance 10^{-13} on the jump of the Robin condition on the interfaces). Numerically, we can thus observe that our estimate $\eta_{\mathrm{dd}}^{k,m}$ is an upper bound on the space-time DD error, though we have no theoretical proof for this.

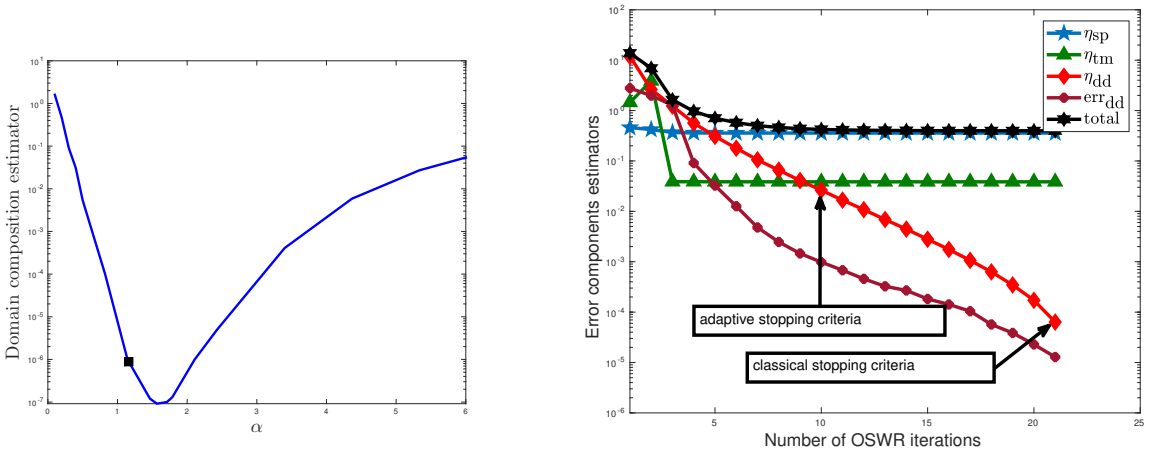

FIGURE 9.3. Example 1: Domain decomposition estimator $\eta_{\mathrm{dd}}^{k,m}$ after 25 Robin–OSWR iterations as a function of the parameter α (left) and evolution of the spatial, temporal, and domain decomposition estimators as a function of the number of Robin–OSWR iterations until $\mathrm{err}_{\mathrm{OSWR}}^{21} \leq 10^{-6}$ (right)

Fig. 9.4 next depicts the evolution of the estimated error after using the stopping criteria (8.2) with $\delta_{\mathrm{dd}} = 0.1$ and (8.1) with $\delta_{\mathrm{lin}} = 0.1$. We notice that the error distribution follows the saturation front but also that some error can still be detected near the interface. In Fig. 9.5, the domain decomposition error is shown at two different time steps, and clearly one sees that the DD error does not affect the total error, in agreement with (8.2).

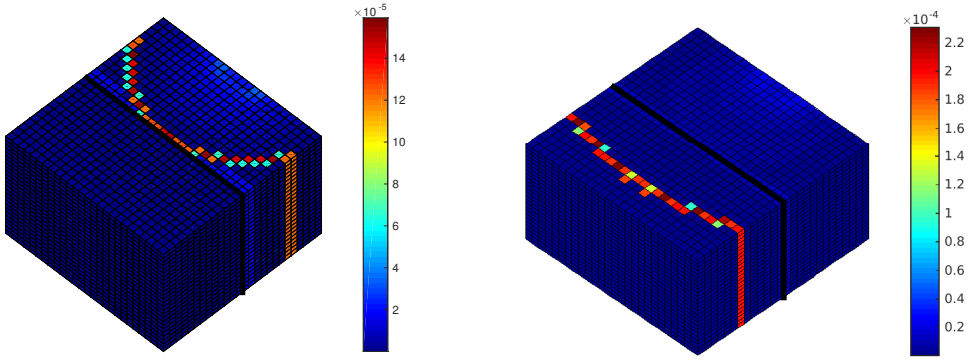

FIGURE 9.4. Example 1: Robin interface conditions, estimated total error for $t = 6.6$ and $t = 15$

Fig. 9.6 finally plots the different estimators in each subdomain, as a function of the Newton iteration at the final iteration of the OSWR algorithm. Only three iterations are required to reach (8.1) for the subdomain solvers, while 9 iterations for the solves in Ω_1 and 6 in Ω_2 are needed to reach the classical criteria (9.3).

9.1.2. *Comparison of the Robin– and Ventcell–OSWR algorithms with adaptive stopping criteria*

We now consider the OSWR algorithm with the two-sided Robin transmission conditions (i.e. $\gamma_{12} = \gamma_{21} = 0$ and $\alpha_{12} \neq \alpha_{21}$) on the one hand, and the Ventcell transmission conditions (i.e. $\gamma = \gamma_{12} = \gamma_{21}$ and $\alpha = \alpha_2 = \alpha_{21}$) on the other hand. Fig. 9.7 shows, for each method, the different estimators

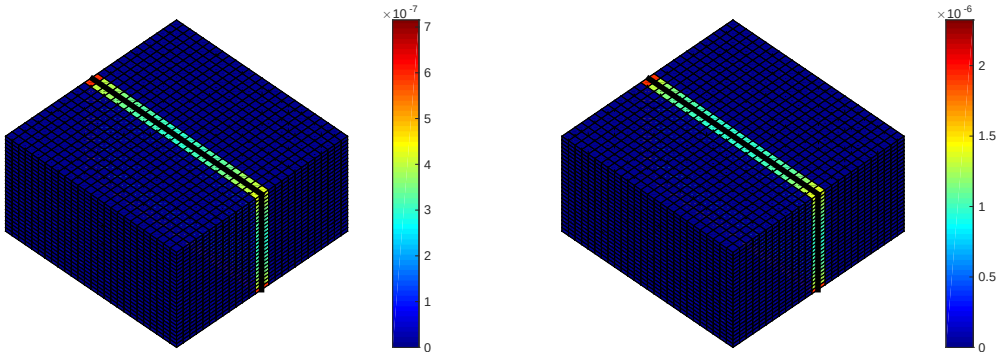

FIGURE 9.5. Example 1: Robin interface conditions, estimated DD error for $t = 6.6$ and $t = 15$

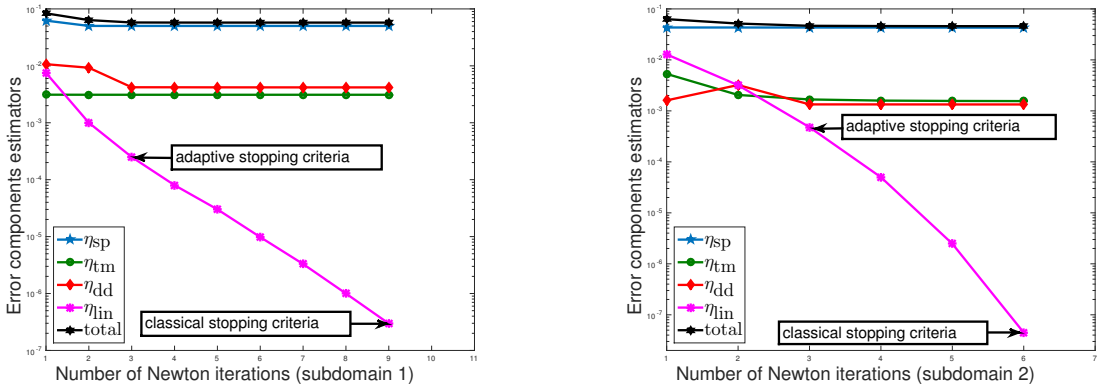

FIGURE 9.6. Example 1: Robin interface conditions, evolution of the spatial, temporal, domain decomposition, and linearization error estimators as a function of Newton iterations for the final iteration of OSWR algorithm for $t = 6.6$; subdomain 1 (left) and subdomain 2 (right)

as a function of the number of DD iterations. We observe that the estimated space and time errors coincide for the two methods and that they are also very close to those obtained with the one-sided Robin–OSWR algorithm (see Fig. 9.3), as expected. For the DD error, both methods are faster than the one-sided Robin–OSWR method. The usual stopping criteria are reached after 10 and 7 iterations, respectively, whereas only 4 iterations are needed with the adaptive stopping criteria (8.2). Fig. 9.8 shows contour lines of the DD estimator $\eta_{\text{dd}}^{k,m}$ as a function of the parameters, at the final OSWR iteration. The square marks the parameters obtained via the optimization procedure described in Remark 3.1. The square corresponds also to $\text{err}_{\text{OSWR}}^4 \approx 1.9 \cdot 10^{-3}$ for the Robin–OSWR method and $\text{err}_{\text{OSWR}}^3 \approx 2.15 \cdot 10^{-4}$ for the Ventcell–OSWR method. It is worth noting that this optimized parameter is close to the parameter that numerically minimizes the error estimate $\eta_{\text{dd}}^{k,m}$.

We have also checked the efficiency of the adaptive linearization stopping criterion (8.1) for both methods. The results (not shown here) are similar to the one-sided Robin–OSWR case, which allows to stop the Newton algorithm after 4 iterations for most of the solves, instead of $7-10$ and $11-14$, respectively, for the classical criterion (9.3).

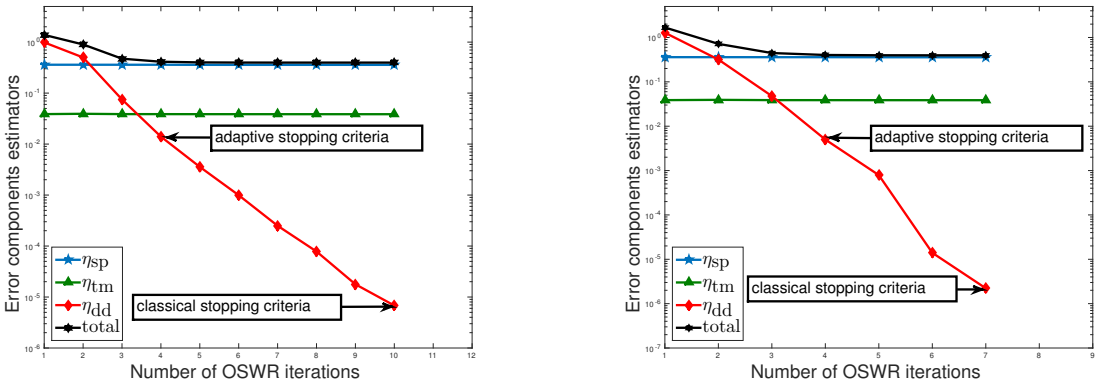

FIGURE 9.7. Example 1: Spatial, temporal, and domain decomposition error estimators as a function of OSWR iterations for the two-sided Robin–OSWR method (left) and the Ventcell–OSWR method (right)

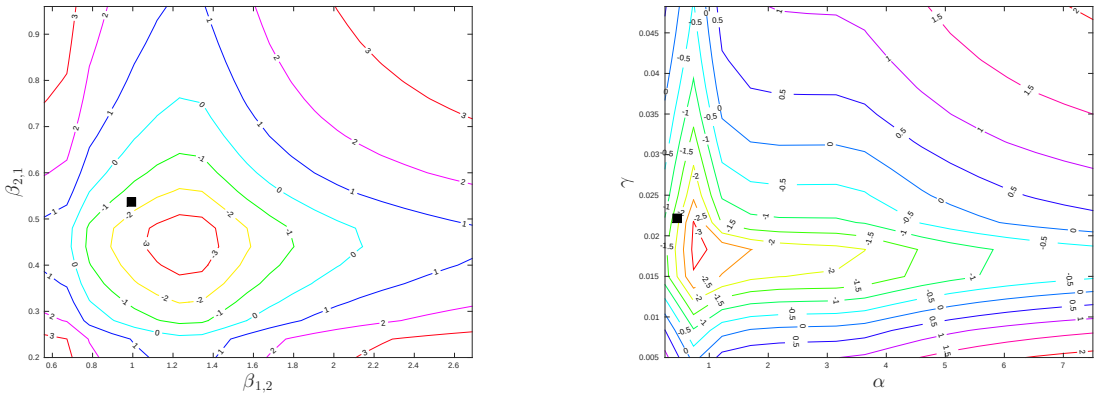

FIGURE 9.8. Example 1: Domain decomposition error estimator $\eta_{\mathrm{dd}}^{k,m}$ as a function of the free parameters after 4 iterations of the OSWR of the two-sided Robin–OSWR method (left) and 3 iterations of the optimized Ventcell–OSWR method (right)

9.2. **Example 2: DNAPL infiltration in a low capillarity lens**

We consider a DNAPL infiltration problem with two different rock types, inspired from [34]. We take $\Omega = (0,1)^3$ and $T = 4 \cdot 10^2$. The medium contains a lens with different capillary pressure curve. The gas and water mobilities depend only on space and are given by $\lambda_1(u) = 1/4$, $\lambda_2(u) = 2/3$, and the capillary pressure curves have the form (see Fig. 9.9)

$$\pi_1(u) = -\ln(1-u), \quad \text{and} \quad \pi_2(u) = -(0.5 + \ln(1-u)).$$

The gas is injected along one side of the domain and a Dirichlet condition is imposed on the opposite face, while no-flow boundary conditions are imposed on the remaining faces. We use a uniform mesh with 17576 elements (corresponding to 26 elements in each layer of each direction).

The time interval $[0, T]$ is decomposed into 8 equal time windows. The OSWR algorithm is employed over each time window until the stopping criteria (8.2) is satisfied, and then the next time window is treated by the DD algorithm. For this example, we use the 2-sided Robin–OSWR method. The Robin

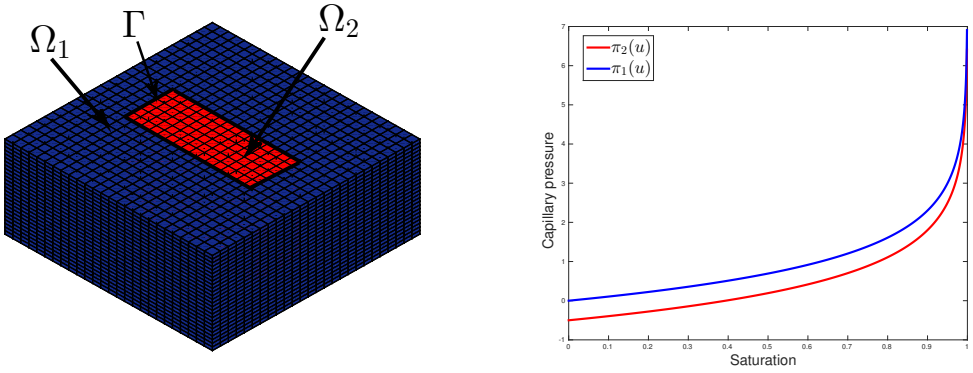

FIGURE 9.9. Example 2: geometry and mesh (left), capillary pressure functions (right)

parameters are calculated using the same procedure as in the first example for the first time window, and we keep the same optimized parameters for all time windows.

Fig. 9.10 shows the evolution of the saturation over the whole domain. In this experiment, the flow is driven by the difference in the capillary pressures. In contrast to the previous example, when the gas reaches the interface, the flow crosses immediately the interface through the domain Ω_2 and the gas accumulates into the lens as the capillary pressure remains discontinuous. The gas inside rock type 2 snakes around the interface to travel again through rock type 1 and then starts to spread into the surrounding medium when the entry pressure given by $\pi_1(0) = 0$ is reached. In fact, the lens acts as a capillary trap as it is much easier for the gas to enter the lens than to leave it, because of the difference in capillary pressures.

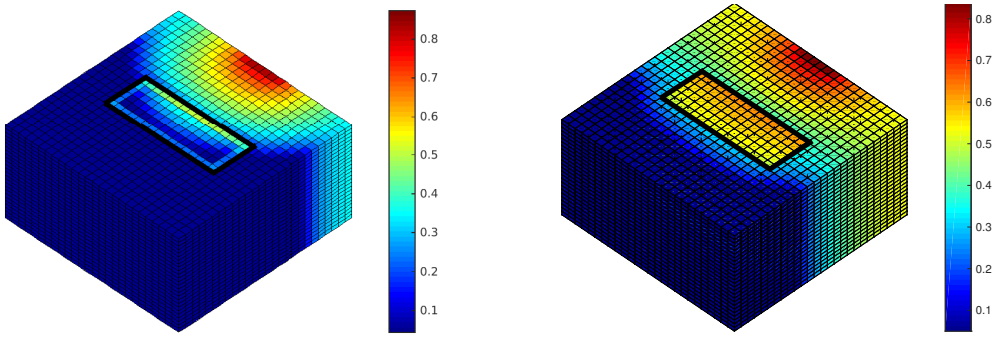

FIGURE 9.10. Example 2: saturation, for $t = 1.5 \cdot 10^2$ and $t = 4 \cdot 10^2$

We come now to the analysis of the OSWR algorithm. In Fig. 9.11, we plot the different estimators as functions of the OSWR iterations for the first, fifth, and final time windows. The classical OSWR algorithm needs 49 iterations overall to converge, with 7 iterations for the first time window, and then between 5 and 7 iterations for the remaining ones. The adaptive OSWR needs 5 iterations to reach the DD stopping criteria for the first time window, and then 2 or 3 iterations for the remaining ones, see Fig 9.12 (left) for the details, and 24 in total. The adaptive linearization stopping criterion (8.1) is also an efficient way of stopping the Newton iterations. In Fig. 9.12 (right), we plot the cumulative number of Newton iterations for the last OSWR iteration. In average, the adaptive stopping criteria reduce the number of Newton iterations from 15.9 to 8.3.

In Fig. 9.13, we plot the evolution of the estimates, using the stopping criteria (8.2) with $\delta_{\text{dd}} = 0.1$ and (8.1) with $\delta_{\text{lin}} = 0.1$. As for the previous example, again the distribution follows the saturation front and also renders some error near the interface.

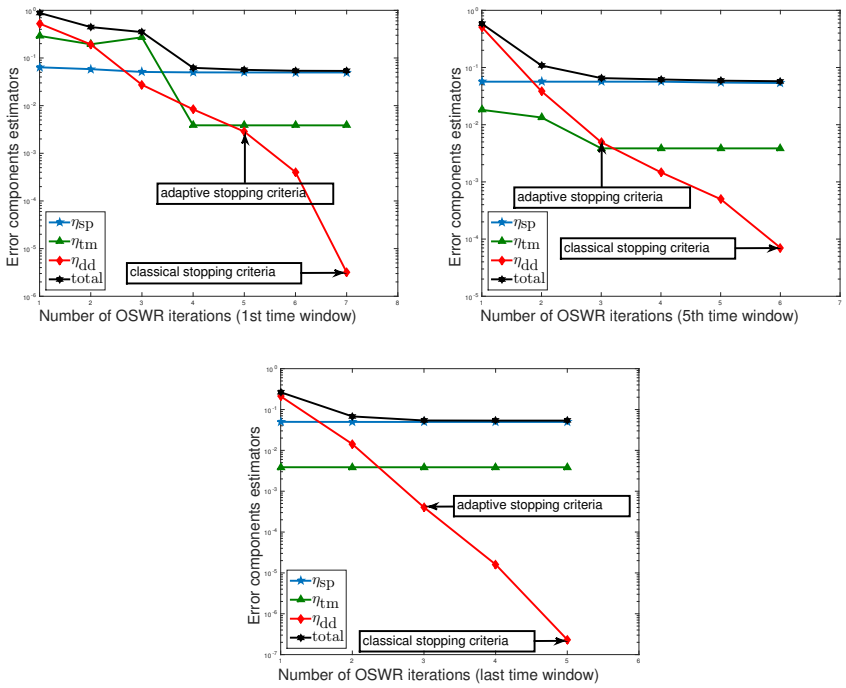

Figure 9.11. Example 2: evolution of the spatial, temporal, and domain decomposition error estimators as a function of the number of Robin–OSWR iterations for the first (left), fifth (middle), and last (right) time windows

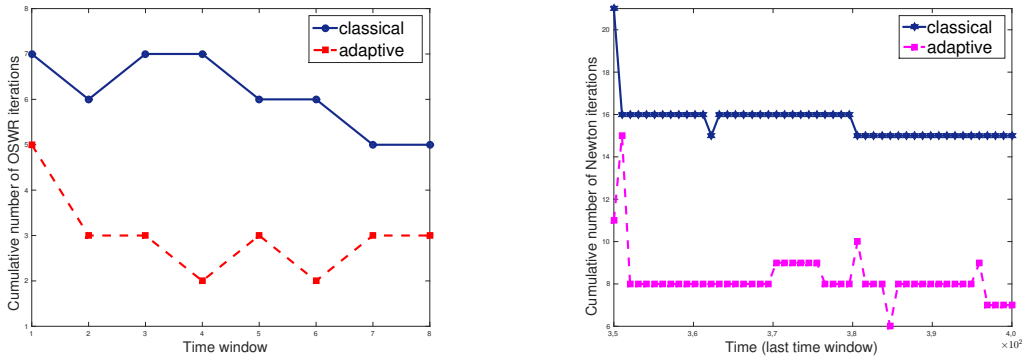

Figure 9.12. Example 2: The cumulative number of OSWR iterations as a function of time windows (left) and the cumulative number of Newton iterations for the last OSWR iteration (last window) as a function of time (right)

9.3. **Example 3: injection along a discontinuity**

We consider a numerical experiment from [5] given by the displacement of a non-wetting fluid by a wetting fluid in a domain made up of two regions with different rock types. The domain is taken as $\Omega = (0, 10)^3$ and the final time is $T = 400$. The injection boundary is taken orthogonal to the interface Γ which makes the flow parallel to the discontinuity and compete in the two subdomains to reach the production boundary on the opposite side. In this example, the capillary pressure functions and the

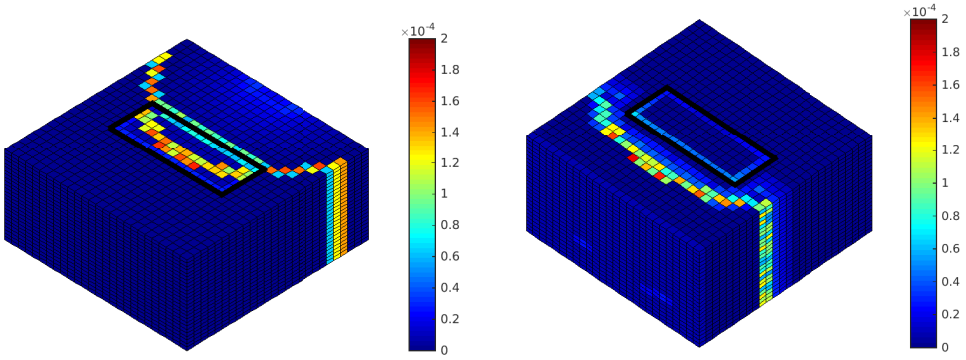

FIGURE 9.13. Example 2: estimated total error for $t = 1.5 \cdot 10^2$ and $t = 4 \cdot 10^2$

phase mobilities are given by the widely used van Genuchten model [53], i.e.,

$$\pi_i(u) = P_i\big((1-u)^{-1/\mu} - 1\big)^{1/\nu},$$

and

$$\lambda_{\mathrm{w}}(u) = \sqrt{u}[1-(1-u^{\nu})^{\mu}]^2, \quad \text{and} \quad \lambda_{\mathrm{g}}(u) = (1-u)^2(1-u^{\nu})^{2\mu},$$

with $\nu = 2.8$, $\mu = 1 - 1/\nu$, and P_1 and P_2 two constants depending on the rock parameters. We take $P_1 = 10$ and $P_2 = 5$. Implicitly, this choice implies that rock type 1 is two times more permeable than rock type 2. Contrarily to the previous test cases, the capillary pressure functions are now matching between the two rock types, see Fig. 9.14 (left) (cf. also condition (2.3) and Remark 6.2).

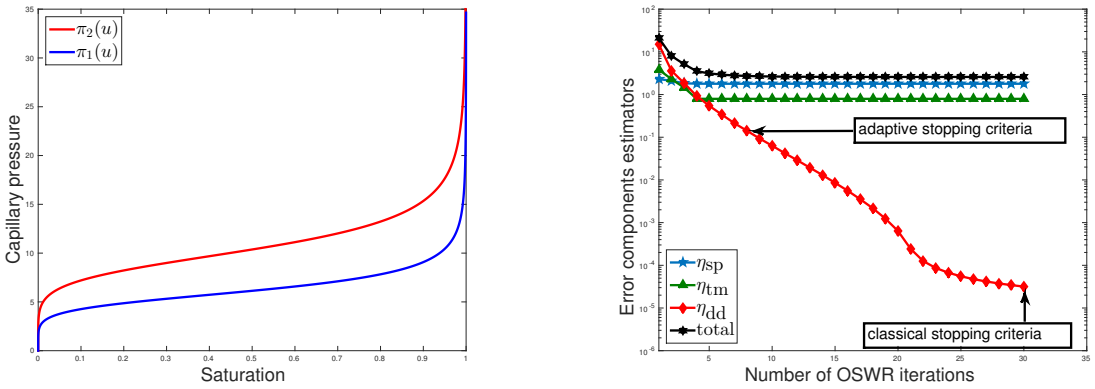

FIGURE 9.14. Example 3: capillary pressure functions (left) and evolution of the spatial, temporal, and domain decomposition estimators as a function of the number of Robin–OSWR iterations (right)

The initial saturation is set equal to 0.05 in rock 1 while in rock 2, it is set so as to satisfy the equality of capillary pressure on the interface. We use Robin–OSWR method for this example. The saturation and the capillary pressure are shown at the final time in Fig. 9.15, and one can see that the saturation is discontinuous across the interface, but that the capillary pressure is continuous. One can also see that because of the contrast in the capillary pressure field, the saturation front moves faster inside rock 2, allowing for a discontinuous change in saturation at the interface.

In Fig. 9.14 (right), we plot the different estimators as functions of the OSWR iterations when using the stopping criteria (8.2) with $\delta_{\mathrm{dd}} = 0.1$ and (8.1) with $\delta_{\mathrm{lin}} = 0.1$. The non-adaptive OSWR needs 30

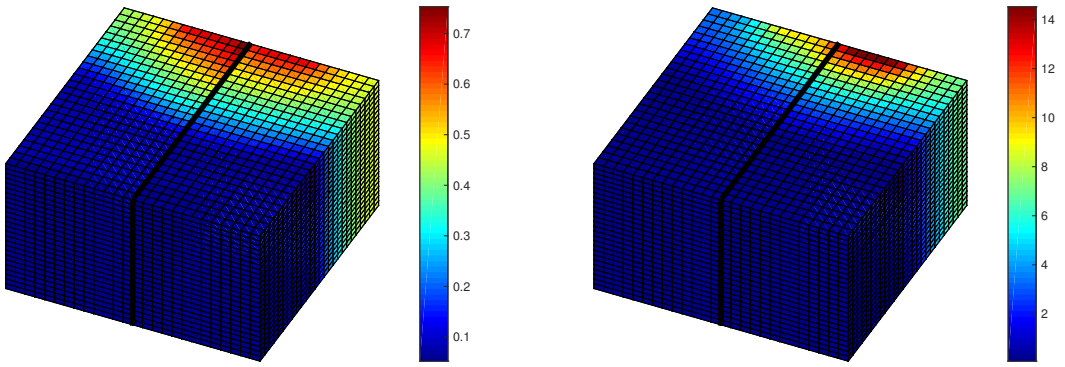

Figure 9.15. Example 3: saturation (left) and capillary pressure (right) at final time

iterations to satisfy (9.3), while the adaptive OSWR only needs 8 iterations. Regarding the efficiency of the adaptive linearization stopping criterion (8.1), we observed that more than 2/3 of the Newton iterations needed to reach the classical linearization stopping criterion (9.3) can be sparred.

Finally, in Fig. 9.16, the total error as well as the domain decomposition error are shown shown at the final time step. Again, as expected, the DD error does not affect the total error. Particularly, the error follows the saturation front which is discontinuous across the interface. Also, some space error on both sides of the interface and near the injection boundary can still be detected.

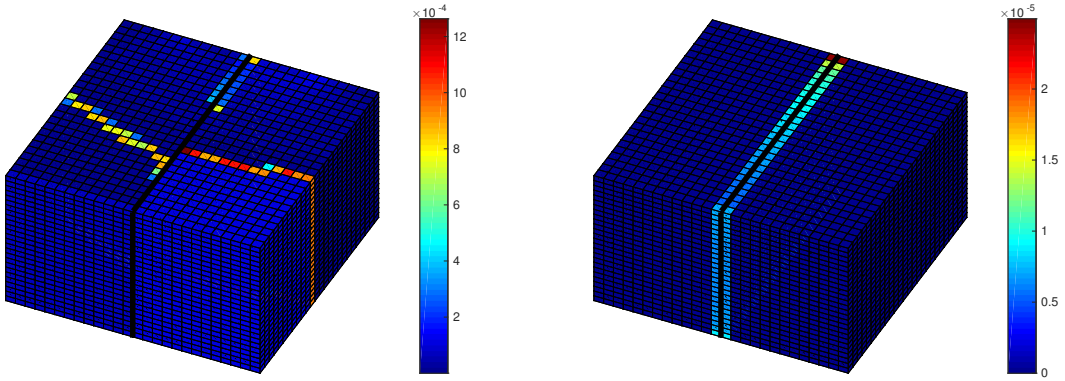

Figure 9.16. Example 3: estimated total error (left) and domain decomposition error (right) at final time

10. **Conclusion**

We proposed an adaptive domain decomposition algorithm that is global-in-time and works as follows:

(1) At each DD iteration, the problem is solved independently in each subdomain on the whole time interval, and then Robin or Ventcell boundary data are exchanged across the space-time interface.

(2) During the DD iteration and at each time and linearization steps, several estimators are computed. Then, the error induced by domain decomposition can be compared to that coming from linearization and spatial and temporal discretizations. The iterations are stopped when the DD estimator becomes smaller (up to a user-chosen constant) than the other error components.

The results confirm that this approach is applicable to the present degenerate parabolic problem with nonlinear and discontinuous transmission conditions. In particular, the DD estimator is a practical tool to estimate the DD error component, and combining optimized parameters and adaptive stopping criteria results in efficient OSWR algorithms. As a benefit, moreover, the overall error is guaranteed to lie below the computed overall estimate.

Appendix A. Details on the equilibrated flux reconstruction

We provide here the details on the reconstruction of an equilibrated flux satisfying (5.3), following closely [6, 7]. For each subdomain Ω_i, we consider a subset B_i of Ω_i, termed a band, which contains all the elements of $\mathcal{T}_{h,i}$ that share a face, and edge, on a point with the interface Γ. We denote by $\mathcal{T}_{h,i}^B$ the corresponding submesh. We start from $-\nabla\varphi_{h,i}^{k,n,m}$ given by (5.4a), which is subdomain-wise $\mathbf{H}(\mathrm{div})$-conforming (belongs to $\mathbf{RTN}_0(\Omega_i)$), $i=1,2$ and set

$$\boldsymbol{\sigma}_h^{k,n,m}|_K := -\nabla\varphi_{h,i}^{k,n,m}|_K, \quad \forall K\in\mathcal{T}_{h,i} \text{ s.t. } K\notin\mathcal{T}_{h,i}^B. \tag{A.1}$$

In the bands, we will modify $-\nabla\varphi_{h,i}^{k,n,m}$ so as to arrive at (5.3); note that simply prescribing the normal components of $\boldsymbol{\sigma}_h^{k,n,m}$ by $\{\!\{-\nabla\varphi_{h,i}^{k,n,m}\cdot\mathbf{n}_{B_i}\}\!\}$ at the interface would lead to (5.3a) but not to (5.3b). We denote by Γ_i^b the boundaries (in 3D for the situation of Fig. A.1, $b=1,2,3,4$) of ∂B_i that intersect $\partial\Omega$, for $i=1,2$. We denote also by Γ_i^{int} the boundary of ∂B_i that is inside Ω_i, $i=1,2$, see Fig. A.1. We then identify nine corrections $\left(c_{\Gamma_1^b}^{k,n,m}\right)_{1\le b\le 4}$, $\left(c_{\Gamma_2^b}^{k,n,m}\right)_{1\le b\le 4}$, and $c_\Gamma^{k,n,m}$ to the averaged

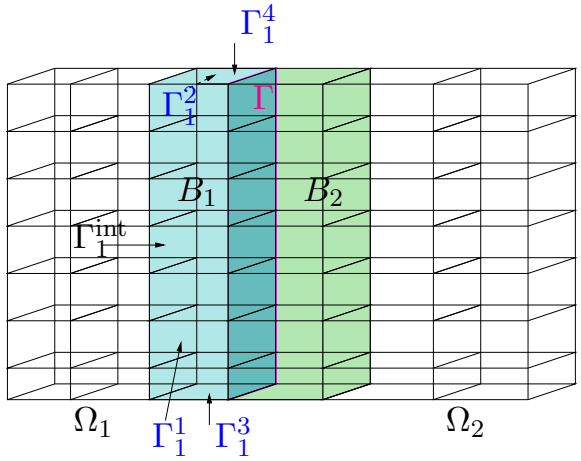

FIGURE A.1. Bands B_1 and B_2 surrounding the interface Γ in three space dimensions

flux $\{\!\{-\nabla\varphi_{h,i}^{k,n,m}\cdot\mathbf{n}_{B_i}\}\!\}$ that will lead to equilibrium in each band B_i, $i=1,2$. In other words, we seek to satisfy the two balancing conditions, for $i=1,2$:

$$\sum_{b=1}^{4} c_{\Gamma_i^b}^{k,n,m} + (\mathbf{n}_\Gamma\cdot\mathbf{n}_{B_i})c_\Gamma^{k,n,m} = \left(f_i^n - \frac{u_K^{k,n,m}-u_K^{k,n-1}}{\tau^n},1\right)_{B_i} - (\{\!\{-\nabla\varphi_{h,i}^{k,n,m}\cdot\mathbf{n}_{B_i}\}\!\},1)_{\partial B_i}. \tag{A.2}$$

Here $\mathbf{n}_\Gamma$ is a unit vector normal to Γ, pointing either from Ω_1 to Ω_2, or from Ω_2 to Ω_1, and $\mathbf{n}_{B_i}$ is the outward unit vector normal to ∂B_i.

The *coarse interface problem* (A.2) is solved via the *least squares minimization*, see [7] for the details. Finally, the corrections are distributed from the boundary of the bands to their interiors by approximating, using the mixed finite element or the finite volume method, the following local Neumann problems: find $(q_{h,i}^{k,n,m}, \boldsymbol{\sigma}_{h,i}^{k,n,m}) \in \mathbb{P}_0(\mathcal{T}_{h,i}^B) \times \mathbf{RTN}_0(B_i)$ with $(q_{h,i}^{k,n,m}, 1)_{B_i} = 0$ such that

$$\begin{cases} \nabla\cdot\boldsymbol{\sigma}_{h,B_i}^{k,n,m}|_K = f_i^n|_K - \dfrac{u_K^{k,n,m} - u_K^{k,n-1}}{\tau^n} & \forall K \in \mathcal{T}_{h,i}^B, \\ \boldsymbol{\sigma}_{h,B_i}^{k,n,m} + \nabla\varphi_{h,i}^{k,n,m} = -\nabla q_{h,i}^{k,n,m}, & \text{in appropriate weak sense in } B_i, \\ \boldsymbol{\sigma}_{h,B_i}^{k,n,m}\cdot\mathbf{n}_\Gamma = -\nabla\varphi_{h,i}^{k,n,m}\cdot\mathbf{n}_\Gamma, & \text{on } \Gamma_i^{\text{int}}, \\ \boldsymbol{\sigma}_{h,B_i}^{k,n,m}\cdot\mathbf{n}_\Gamma = \{\!\{-\nabla\varphi_{h,i}^{k,n,m}\cdot\mathbf{n}_\Gamma\}\!\} + \dfrac{1}{|\Gamma|}c_\Gamma^{k,n,m}, & \text{on } \Gamma, \\ \boldsymbol{\sigma}_{h,B_i}^{k,n,m}\cdot\mathbf{n}_\Gamma = -\nabla\varphi_{h,i}^{k,n,m}\cdot\mathbf{n}_\Gamma + \dfrac{1}{|\Gamma_i^b|}c_{\Gamma_i^b}^{k,n,m}, & \text{on } \Gamma_i^b. \end{cases}$$

We finally complement (A.1) by setting $\boldsymbol{\sigma}_h^{k,n,m}|_{B_i} := \boldsymbol{\sigma}_{h,B_i}^{k,n,m}$.

Acknowledgments

This work is the result of a collaboration that took place during the CEMRACS summer school & projects 2016. We warmly thank the organizers as well as the CIRM for its welcome.

References

[1] Elyes Ahmed, Sarah Ali Hassan, Caroline Japhet, Michel Kern, and Martin Vohralík. A posteriori error estimates and stopping criteria for space-time domain decomposition for two-phase flow between different rock types. `https://hal.inria.fr/hal-01540956`, 2017.

[2] Elyes Ahmed, Jérôme Jaffré, and Jean E. Roberts. A reduced fracture model for two-phase flow with different rock types. *Math. Comput. Simulation*, 137:49–70, 2017.

[3] Elyes Ahmed, Caroline Japhet, and Michel Kern. Global-in-time domain decomposition for a nonlinear diffusion problem. `https://hal.inria.fr/hal-02263280`, accepted in the Proceedings of the 25th International Conference on Domain Decomposition Methods, 2019.

[4] Elyes Ahmed, Caroline Japhet, and Michel Kern. Space-time domain decomposition for two-phase flow between different rock types. `https://hal.inria.fr/hal-02275690`, 2019.

[5] Clarisse Alboin, Jérôme Jaffré, Jean E. Roberts, Xuewen Wang, and Christophe Serres. Domain decomposition for some transmission problems in flow in porous media. In *Numerical treatment of multiphase flows in porous media (Beijing, 1999)*, volume 552 of *Lecture Notes in Physics*, pages 22–34. Springer, 2000.

[6] Sarah Ali Hassan, Caroline Japhet, Michel Kern, and Martin Vohralík. A posteriori stopping criteria for optimized Schwarz domain decomposition algorithms in mixed formulations. *Comput. Methods Appl. Math.*, 18(3):495–519, 2018.

[7] Sarah Ali Hassan, Caroline Japhet, and Martin Vohralík. A posteriori stopping criteria for space-time domain decomposition for the heat equation in mixed formulations. *Electron. Trans. Numer. Anal.*, 49:151–181, 2018.

[8] Boris Andreianov, Konstantin Brenner, and Clément Cancès. Approximating the vanishing capillarity limit of two-phase flow in multi-dimensional heterogeneous porous medium. *ZAMM, Z. Angew. Math. Mech.*, 94(7-8):655–667, 2014.

[9] Mario Arioli, Daniel Loghin, and Andrew J. Wathen. Stopping criteria for iterations in finite element methods. *Numer. Math.*, 99(3):381–410, 2005.

[10] Khalid Aziz and Antonín Settari. *Petroleum Reservoir Simulation*. Applied Science Publishers, 1979.

[11] Roland Becker, Claes Johnson, and Rolf Rannacher. Adaptive error control for multigrid finite element methods. *Computing*, 55(4):271–288, 1995.

[12] Daniel Bennequin, Martin J. Gander, and Laurence Halpern. A homographic best approximation problem with application to optimized Schwarz waveform relaxation. *Math. Comput.*, 78(265):185–223, 2009.

[13] Heiko Berninger, Sébastien Loisel, and Oliver Sander. The 2-Lagrange multiplier method applied to nonlinear transmission problems for the Richards equation in heterogeneous soil with cross points. *SIAM J. Sci. Comput.*, 36(5):A2166–A2198, 2014.

[14] Michiel Bertsch, Roberta Dal Passo, and Cornelis J. Van Duijn. Analysis of oil trapping in porous media flow. *SIAM J. Math. Anal.*, 35(1):245–267, 2003.

[15] Konstantin Brenner, Clément Cancès, and Danielle Hilhorst. Finite volume approximation for an immiscible two-phase flow in porous media with discontinuous capillary pressure. *Comput. Geosci.*, 17(3):573–597, 2013.

[16] Filipa Caetano, Martin J. Gander, Laurence Halpern, and Jérémie Szeftel. Schwarz waveform relaxation algorithms for semilinear reaction-diffusion equations. *Netw. Heterog. Media*, 5(3):487–505, 2010.

[17] Clément Cancès. Nonlinear parabolic equations with spatial discontinuities. *NoDEA, Nonlinear Differ. Equ. Appl.*, 15(4-5):427–456, 2008.

[18] Clément Cancès. Finite volume scheme for two-phase flows in heterogeneous porous media involving capillary pressure discontinuities. *M2AN Math. Model. Numer. Anal.*, 43(5):973–1001, 2009.

[19] Clément Cancès, Thierry Gallouët, and Alessio Porretta. Two-phase flows involving capillary barriers in heterogeneous porous media. *Interfaces Free Bound.*, 11(2):239–258, 2009.

[20] Clément Cancès, Iuliu Sorin Pop, and Martin Vohralík. An a posteriori error estimate for vertex-centered finite volume discretizations of immiscible incompressible two-phase flow. *Math. Comput.*, 83(285):153–188, 2014.

[21] Guy Chavent and Jérôme Jaffré. *Mathematical models and finite elements for reservoir simulation*, volume 17 of *Studies in Mathematics and Its Applications*. North-Holland, 1986.

[22] Daniele A. Di Pietro, Eric Flauraud, Martin Vohralík, and Soleiman Yousef. A posteriori error estimates, stopping criteria, and adaptivity for multiphase compositional Darcy flows in porous media. *J. Comput. Phys.*, 276:163–187, 2014.

[23] Daniele A. Di Pietro, Martin Vohralík, and Soleiman Yousef. Adaptive regularization, linearization, and discretization and a posteriori error control for the two-phase Stefan problem. *Math. Comput.*, 84(291):153–186, 2015.

[24] Guillaume Enchéry, R. Eymard, and Anthony Michel. Numerical approximation of a two-phase flow problem in a porous medium with discontinuous capillary forces. *SIAM J. Numer. Anal.*, 43(6):2402–2422, 2006.

[25] Alexandre Ern and Martin Vohralík. A posteriori error estimation based on potential and flux reconstruction for the heat equation. *SIAM J. Numer. Anal.*, 48(1):198–223, 2010.

[26] Alexandre Ern and Martin Vohralík. Adaptive inexact Newton methods with a posteriori stopping criteria for nonlinear diffusion PDEs. *SIAM J. Sci. Comput.*, 35(4):A1761–A1791, 2013.

[27] Robert Eymard, Thierry Gallouët, and Raphaèle Herbin. Finite volume methods. In *Handbook of Numerical Analysis, Vol. VII*, pages 713–1020. North-Holland, 2000.

[28] Robert Eymard, Thierry Gallouët, and Raphaèle Herbin. Finite volume approximation of elliptic problems and convergence of an approximate gradient. *Appl. Numer. Math.*, 37(1-2):31–53, 2001.

[29] Martin J. Gander. Optimized Schwarz methods. *SIAM J. Numer. Anal.*, 44(2):699–731, 2006.

[30] Martin J. Gander, Laurence Halpern, and Frédéric Nataf. Optimal Schwarz waveform relaxation for the one dimensional wave equation. *SIAM J. Numer. Anal.*, 41(5):1643–1681, 2003.

[31] Benjamin Ganis, Kundan Kumar, Gergina Pencheva, Mary F. Wheeler, and Ivan Yotov. A global Jacobian method for mortar discretizations of a fully implicit two-phase flow model. *Multiscale Model. Simul.*, 12(4):1401–1423, 2014.

[32] Florian Haeberlein, Laurence Halpern, and Anthony Michel. Newton-Schwarz optimised waveform relaxation Krylov accelerators for nonlinear reactive transport. In *Domain decomposition methods in science and engineering XX*, volume 91 of *Lect. Notes Comput. Sci. Eng.*, pages 387–394. Springer, 2013.

[33] Laurence Halpern and Florence Hubert. A finite volume Ventcell-Schwarz algorithm for advection-diffusion equations. *SIAM J. Numer. Anal.*, 52(3):1269–1291, 2014.

[34] Rainer Helmig. *Multiphase Flow and Transport Processes in the Subsurface*. Springer, 1997.

[35] Thi-Thao-Phuong Hoang, Jérôme Jaffré, Caroline Japhet, Michel Kern, and Jean E. Roberts. Space-time domain decomposition methods for diffusion problems in mixed formulations. *SIAM J. Numer. Anal.*, 51(6):3532–3559, 2013.

[36] Thi-Thao-Phuong Hoang, Caroline Japhet, Michel Kern, and Jean E. Roberts. Ventcell conditions with mixed formulations for flow in porous media. In T. Dickopf, Martin J. Gander, L. Halpern, R. Krause, and L. F. Pavarino, editors, *Decomposition Methods in Science and Engineering XXII*, volume 104 of *Lecture Notes in Computational Science and Engineering*, pages 531–540. Springer, 2016.

[37] Caroline Japhet and Frédéric Nataf. The best interface conditions for domain decomposition methods: absorbing boundary conditions. In *Absorbing Boundaries and Layers, Domain Decomposition Methods*, pages 348–373. Nova Sci. Publ., 2001.

[38] Pavel Jiránek, Zdeněk Strakoš, and Martin Vohralík. A posteriori error estimates including algebraic error and stopping criteria for iterative solvers. *SIAM J. Sci. Comput.*, 32(3):1567–1590, 2010.

[39] Hanyu Li and Mary F. Wheeler. Sequential Refinement Solver using Space-Time Domain Decomposition for Non-linear Multiphase Flow Problems. `https://arxiv.org/abs/1901.09436`, 2019.

[40] Knut-Andreas Lie, Stein Krogstad, Ingeborg S. Ligaarden, Jostein R. Natvig, Halvor M. Nilsen, and Bård Skaflestad. Open source MATLAB implementation of consistent discretisations on complex grids. *Comput. Geosci.*, 16(2):297–322, 2012.

[41] Véronique Martin. An optimized Schwarz waveform relaxation method for the unsteady convection diffusion equation in two dimensions. *Appl. Numer. Math.*, 52(4):401–428, 2005.

[42] Ricardo H. Nochetto, Alfred Schmidt, and Claudio Verdi. A posteriori error estimation and adaptivity for degenerate parabolic problems. *Math. Comput.*, 69(229):1–24, 2000.

[43] Jan Papež, Ulrich Rüde, Martin Vohralík, and Barbara Wohlmuth. Sharp algebraic and total a posteriori error bounds for h and p finite elements via a multilevel approach. `https://hal.inria.fr/hal-01662944`, submitted for publication, 2017.

[44] Jan Papež, Zdeněk Strakoš, and Martin Vohralík. Estimating and localizing the algebraic and total numerical errors using flux reconstructions. *Numer. Math.*, 138(3):681–721, 2018.

[45] Gergina Pencheva, Martin Vohralík, Mary F. Wheeler, and Tim Wildey. Robust a posteriori error control and adaptivity for multiscale, multinumerics, and mortar coupling. *SIAM J. Numer. Anal.*, 51(1):526–554, 2013.

[46] Valentine Rey, Pierre Gosselet, and Christian Rey. Strict lower bounds with separation of sources of error in non-overlapping domain decomposition methods. *Internat. J. Numer. Methods Engrg.*, 108(9):1007–1029, 2016.

[47] Valentine Rey, Christian Rey, and Pierre Gosselet. A strict error bound with separated contributions of the discretization and of the iterative solver in non-overlapping domain decomposition methods. *Comput. Methods Appl. Mech. Engrg.*, 270:293–303, 2014.

[48] David Seus, Koondanibha Mitra, Iuliu Sorin Pop, Florin Adrian Radu, and Christian Rohde. A linear domain decomposition method for partially saturated flow in porous media. *Comput. Methods Appl. Mech. Engrg.*, 333:331–355, 2018.

[49] Gurpreet Singh and Mary F. Wheeler. A space-time domain decomposition approach using enhanced velocity mixed finite element method. *J. Comput. Phys.*, 374:893–911, 2018.

[50] Jan Ole Skogestad, Eirik Keilegavlen, and Jan M. Nordbotten. Domain decomposition strategies for nonlinear flow problems in porous media. *J. Comput. Phys.*, 234:439–451, 2013.

[51] Jan Ole Skogestad, Eirik Keilegavlen, and Jan M. Nordbotten. Two-scale preconditioning for two-phase nonlinear flows in porous media. *Transp. Porous Media*, 114(2):485–503, 2016.

[52] Cornelis J. van Duijn, Johannes Molenaar, and M. J. de Neef. The effect of capillary forces on immiscible two-phase flow in heterogeneous porous media. *Transport in Porous Media*, 21(1):71–93, 1995.

[53] Martinus Th. van Genuchten. A closed form for predicting the hydraulic conductivity of unsaturated soils. *Soil Sci. Soc. Amer. J.*, 44:892–898, 1980.

[54] Martin Vohralík and Mary F. Wheeler. A posteriori error estimates, stopping criteria, and adaptivity for two-phase flows. *Comput. Geosci.*, 17(5):789–812, 2013.

[55] Ivan Yotov. A mixed finite element discretization on non-matching multiblock grids for a degenerate parabolic equation arising in porous media flow. *East-West J. Numer. Math.*, 5(3):211–230, 1997.

[56] Ivan Yotov. Interface solvers and preconditioners of domain decomposition type for multiphase flow in multiblock porous media. In *Scientific computing and applications*, volume 7 of *Adv. Comput. Theory Pract.*, pages 157–167. Nova Sci. Publ., Huntington, NY, 2001.